Mechanistic Details of Early Steps in Coenzyme Q Biosynthesis Pathway in Yeast

Laurie-Anne Payet, Mélanie Leroux, John C. Willison, Akio Kihara, Ludovic Pelosi, Fabien Pierrel

Mechanistic Details of Early Steps in Coenzyme Q Biosynthesis Pathway in Yeast.

Laurie-Anne Payet[1,2,3], Mélanie Leroux[3,4†], John C. Willison[4], Akio Kihara[5], Ludovic Pelosi[1,2], Fabien Pierrel[1,2]*

[1] Univ. Grenoble Alpes, Laboratoire Technologies de l'Ingénierie Médicale et de la Complexité – Informatique, Mathématiques et Applications (TIMC-IMAG), F-38000 Grenoble, France.
[2] Centre National de Recherche Scientifique (CNRS), TIMC-IMAG, F-38000 Grenoble, France.
[3]These authors contributed equally to this work
[4] CEA-Grenoble, DRF-BIG-CBM, UMR5249, F-38000 Grenoble, France.
[5] Faculty of Pharmaceutical Sciences, Hokkaido University, Kita 12-jo, Nishi 6-chome, Kita-ku, Sapporo 060-0812, Japan.
* Correspondence : fabien.pierrel@univ-grenoble-alpes.fr

[†] Present address: Centre National de Recherche Scientifique (CNRS) - Univ. Grenoble Alpes, CERMAV, UPR 5301, F-38000 Grenoble, France.

Running title: yeast pathway from tyrosine to coenzyme Q

SUMMARY

Coenzyme Q (Q) is essential for the bioenergetics of heterotrophic eukaryotic cells. However, some aspects of Q biosynthesis are poorly understood, including how 4-hydroxybenzoic acid (4-HB), the precursor of Q, is made. We show that in the yeast *Saccharomyces cerevisiae* grown under conditions limiting for para-aminobenzoic acid, most Q originates from the shikimate pathway or from exogenous tyrosine via a common intermediate, 4-hydroxyphenylpyruvate (4-HPP). We characterize two of the steps from tyrosine to 4-HB: the deamination of tyrosine to 4-HPP, which is catalyzed by the Aro8 and Aro9 proteins, and the oxidation of 4-hydroxybenzaldehyde to 4-HB, which is catalyzed by the aldehyde dehydrogenase Hfd1. Inactivation of the *hfd1* gene in yeast resulted in Q deficiency, which was rescued by the human enzyme ALDH3A1. This suggests that ALDH3A1 may play a role in Q biosynthesis in humans and is a potential target for mutations in patients with undefined Q deficiency.

INTRODUCTION

Heterotrophic eukaryotic cells produce most of their energy via oxidative phosphorylation in mitochondria. The electrochemical gradient used for ATP synthesis is generated by the respiratory chain in which the redox lipid coenzyme Q (Q) transfers electrons between membrane-embedded multiprotein complexes responsible for proton pumping (Genova and Lenaz, 2014; Wang and Hekimi, 2016). Q also functions as a membrane antioxidant and a cofactor of uncoupling proteins (Bentinger et al., 2010). Q is composed of a conserved fully-substituted benzoquinone ring which is attached to a polyisoprenyl tail of various length (six isoprenyl units in *Saccharomyces cerevisiae*, ten units in humans). The initial reaction of Q biosynthesis is catalyzed by the Coq2 protein (Ashby et al., 1992; Forsgren et al., 2004), which conjugates the polyprenyl-pyrophosphate tail with 4-hydroxybenzoic acid (4-HB), the precursor of the benzoquinone ring of Q (Olson and Rudney, 1983) (Figure S1A). Multiple Coq proteins (Coq3-Coq9 in *S. cerevisiae*, Figure S1A) localized in the mitochondrial matrix then modify the aromatic ring of prenyl-4-HB in order to yield Q (Tran and Clarke, 2007; Wang and Hekimi, 2012). Abrogation of Q biosynthesis results in the incapacity of *S. cerevisiae* to grow on media containing non-fermentable carbon sources (Johnson et al., 2005) and is embryonically lethal in mammals (Laredj et al., 2014; Wang and Hekimi, 2012). Human primary coenzyme Q deficiency is caused by mutations in nine genes required for Q biosynthesis and results in clinically heterogeneous diseases which are often improved by Q supplementation (Freyer et al., 2015; Quinzii and Hirano, 2011; Salviati et al., 2012). Q is also used as a dietary supplement and ongoing biotechnological efforts aim at improving Q biosynthesis in various microorganisms (Cluis et al., 2011; Lu et al., 2015; Moriyama et al., 2015; Xu et al., 2016).

Although the synthesis of Q from 4-HB is reasonably well understood (Gonzalez-Mariscal et al., 2014; Wang and Hekimi, 2016), the pathway that produces 4-HB in eukaryotes has remained elusive (Kawamukai, 2016). Tracer experiments performed fifty years ago suggested that animals derive 4-HB from tyrosine and phenylalanine (Phe), although Phe may first be converted into tyrosine (Olson, 1966; Olson et al., 1965). Since then, neither enzymes nor intermediates have been assigned to the pathway from tyrosine to 4-HB. Bacteria are known to employ chorismatases like UbiC or XanB2 to synthesize 4-HB from chorismic acid, an intermediate of the shikimate pathway (Siebert et al., 1994; Zhou et al., 2013) which is widespread in microorganisms (Bentley, 1990). The yeast *S. cerevisiae* possesses the shikimate pathway and is thus believed to synthesize 4-HB from tyrosine and chorismic acid (Clarke,

2000) (Figure S1A). However, no homologs of UbiC or XanB2 have been identified in *S. cerevisiae*; thus a direct conversion of chorismic acid into 4-HB is hypothetical in this organism (Figure S1A). A recent study in the plant *Arabidopsis thaliana* demonstrated that Phe and tyrosine independently contribute to the synthesis of 4-HB, but only the pathway originating from Phe has been partially characterized and shown to involve β-oxidation in peroxisomes (Block et al., 2014). Overall, the metabolic pathway from tyrosine to 4-HB appears to be common to eukaryotes, yet it remains uncharacterized to date.

We and others discovered that *S. cerevisiae* synthesizes Q not only from 4-HB but also from para-aminobenzoic acid (pABA) (Marbois et al., 2010; Pierrel et al., 2010). pABA is a precursor in folate metabolism and is synthesized from chorismic acid via two reactions catalyzed by Abz1 and Abz2 (Figure S1A) (Botet et al., 2007). The use of pABA as a precursor of Q may be restricted to *S. cerevisiae* since *Escherichia coli*, *A. thaliana* and human cells do not incorporate pABA into Q (Block et al., 2014; Xie et al., 2015). pABA is a constituent of the widely used YNB synthetic growth medium and may thereby confer normal Q levels to *S. cerevisiae* cells deficient in 4-HB. In the present study, we used YNB culture medium depleted of pABA to study the pathway from tyrosine to 4-HB. By combining isotopic labelling, chemical analogues supplementation, and forward and reverse genetics, we have elucidated the first and last reactions of this pathway in *S. cerevisiae* and have identified the associated enzymes.

RESULTS

Tyrosine but not Phe is a precursor of Q in *S. cerevisiae*

We previously showed that addition of pABA or 4-HB to YNB medium depleted of pABA increased the Q content of *S. cerevisiae* cells, which demonstrated that endogenously synthesized pABA and 4-HB are limiting for Q biosynthesis (Pierrel et al., 2010). Addition of tyrosine to the growth medium increased the level of Q (Figure S1B), supporting that tyrosine is used as a precursor. Indeed, the mass spectrum of Q from cells grown in the presence of $^{15}N^{13}C_9$-tyrosine was consistent with the incorporation of the 6 aromatic carbon atoms of tyrosine into Q (Figure S1C) and 78% of the Q pool was labelled (Figure 1A). In contrast to *A. thaliana* (Block et al., 2014), *S. cerevisiae* did not convert $^{13}C_9$-Phe to Q (Figure 1A), demonstrating the absence of a pathway from Phe to 4-HB in yeast.

4-HPP is an intermediate in the biosynthesis of 4HB

We then evaluated the impact of mutations in the shikimate pathway (Figure S1A). We found that products of the shikimate pathway compete with exogenous $^{15}N^{13}C_9$-tyrosine for Q biosynthesis since the labelling of Q increased in Δ*aro2* and Δ*tyr1* strains (Figure 1A). Aro8 and Aro9 are two aminotransferases that catalyze the last reaction of the biosynthesis of tyrosine, the conversion of 4-HPP into tyrosine (Figure S1A) (Urrestarazu et al., 1998). We assessed whether Aro8 and Aro9 may catalyze the reverse reaction *in vivo*, the deamination of tyrosine to 4-HPP. The labelling of Q from $^{15}N^{13}C_9$-tyrosine diminished drastically in the Δ*aro8*Δ*aro9* strain compared to WT (Figure 1A), supporting the idea that 4-HPP produced by Aro8 and Aro9 is an intermediate in the biosynthesis of 4-HB. Accordingly, inactivation of both branches of 4-HPP biosynthesis, as in Δ*aro8*Δ*aro9*Δ*tyr1* and Δ*aro8*Δ*aro9*Δ*aro2* cells, diminished Q levels (Figure 1B). These results establish that 4-HPP, originating from the shikimate pathway and from the deamination of tyrosine by Aro8 and Aro9, is an intermediate in the production of 4-HB that is used for Q biosynthesis.

The S241L mutation in *hfd1* causes Q deficiency in Δ*aro2* cells

Next, we reasoned that the inactivation of the shikimate pathway together with a disruption of the biosynthesis of 4-HB from exogenous tyrosine should result in Q deficiency. We therefore used the Δ*aro2* strain in a forward genetic screen with lactate-glycerol (LG) medium, growth on which requires Q. After mutagenesis, we isolated a Δ*aro2-mutA* clone that grew poorly on LG medium unless 4-HB was added (Figure S1D). The Q content of Δ*aro2-mutA* cells was very low compared to that of Δ*aro2* cells and was increased by 4-HB but not by tyrosine (Figure 1C), a result consistent with the inactivation of the tyrosine to 4-HB pathway. Addition of pABA to the growth medium increased Q levels in Δ*aro2* and Δ*aro2-mutA* cells (Figure S1E) but to levels slightly lower than those obtained with 4-HB (Figure 1C). Genetic analysis revealed that the mutation of a single gene caused the phenotype of Δ*aro2-mutA* cells (see Supplemental Experimental Procedures). In order to identify the defective gene, the Δ*aro2-mutA* strain was transformed with a *S. cerevisiae* genomic library and the resulting clones were tested for growth on LG medium. The growth was totally recovered with a plasmid carrying the *HFD1* gene whereas plasmids expressing *COQ2-MVD1* or *ARO2* suppressed only partially the phenotype (Figure 1D). *COQ2-MVD1* increased the Q content of Δ*aro2-mutA* cells, whereas *ARO2* was without an effect (Figure S1F). DNA sequencing of the *HFD1* locus identified a C722T mutation in the Δ*aro2-mutA* strain, causing a S241L mutation in the Hfd1 protein. This result establishes that the *HFD1* gene complements the phenotype of the Δ*aro2-*

mutA strain, whereas *COQ2-MVD1* and *ARO2* behave as high copy suppressors, in agreement with the partial recovery of the respiratory growth (Figure 1D).

Hfd1 belongs to the aldehyde dehydrogenase family (Nakahara et al., 2012) and the importance of S241 for Hfd1 function is supported by its presence within a LELGGKSP sequence that is conserved in several family members (Figure S2A). The LELGGKSP sequence connects the catalytic and NAD binding domains of human ALDH2 and ALDH3A1 (Lang et al., 2012; Parajuli et al., 2014) and we found a similar topology in our homology model of Hfd1 (Figure S2B).

Inactivation of *hfd1* results in Q deficiency

Δ*hfd1* cells were deficient in growth on LG medium unless it was supplemented with 4-HB (Figure 2A). Q levels were decreased ~7 fold in Δ*hfd1* cells compared to WT and increased strongly with 4-HB but not with tyrosine (Figure 2B). Q levels also increased with addition of pABA (Figure 2B). Expression of Hfd1, but not Hfd1-S241L, restored respiratory growth and the Q content of the Δ*hfd1* strain (Figures 2A and 2B), confirming the deleterious effect of the S241L mutation. High copy *COQ2-MVD1* increased the Q content of Δ*hfd1* cells, although not to WT levels, whereas *ARO2* had no effect (Figure 2C). Only 7% of Q was labelled in Δ*hfd1* cells grown with $^{15}N^{13}C_9$-tyrosine (Figure 2D), showing that exogenous tyrosine cannot efficiently supply Q biosynthesis in Δ*hfd1* cells contrary to WT cells (Figure 1A).

S. cerevisiae lacks a chorismatase to convert chorismic acid into 4-HB

Δ*hfd1* cells have a functional shikimate pathway since they are prototrophic for aromatic amino acids (data not shown). Nevertheless, they are deficient in Q (Figure 2B), suggesting that chorismic acid does not supply sufficient 4-HB or pABA for Q biosynthesis (Figure S1A). Indeed, we found that expression of the *E. coli* UbiC protein, which catalyzes the direct aromatization of chorismic acid into 4-HB, robustly increased Q in WT and Δ*hfd1* cells, but not in Δ*aro2*Δ*hfd1* cells that do not produce chorismic acid (Figure 2B). As expected, $^{15}N^{13}C_9$-tyrosine did not label Q produced by Δ*hfd1 + ubiC* cells (Figure 2D). These results demonstrate that *S. cerevisiae* lacks a functional chorismatase enzyme and explain that Δ*hfd1* cells are deficient in Q despite their ability to synthesize chorismic acid.

Endogenous pABA is the predominant precursor of Q in the absence of *hfd1*

The relative influx of pABA and 4-HB into the Q biosynthetic pathway is revealed in a Δ*coq6* strain overexpressing Coq8, which does not synthesize Q but instead accumulates 3-

hexaprenyl-4-aminophenol (4-AP) or 3-hexaprenyl-4-hydroxyphenol (4-HP) depending on whether the precursor used is pABA or 4-HB, respectively (Ozeir et al., 2011; Xie et al., 2012). 4-HP decreased in Δ*coq6*Δ*hfd1* cells compared to Δ*coq6* cells (Figure 2E), reflecting a diminished influx of 4-HB caused by the deletion of *hfd1*. The major contribution to Q biosynthesis of 4-HB over pABA was restored by expression of *HFD1* or *ubiC* which diminished 4-AP and increased 4-HP (Figure 2E). Taken together, our results demonstrate that the inactivation of *hfd1* diminishes the pool of 4-HB available for Q biosynthesis whereas that of pABA remains unaffected. We conclude that Hfd1 acts upstream of 4-HB in the metabolic pathway from tyrosine, since *E. coli* UbiC, which produces 4-HB directly from chorismic acid, increased the levels of both Q (Figure 2B) and 4-HB, as indirectly assessed by measuring 4-HP (Figure 2E). Interestingly, expression of *E. coli* UbiC was also recently found to increases Q level in *Schizosaccharomyces pombe* (Moriyama et al., 2015).

Hfd1 oxidizes 4-Hbz to 4-HB

Hfd1 was recently shown to catalyze the oxidation of hexadecanal to hexadecanoic acid as part of the degradation pathway of the sphingoid base dihydrosphingosine (Nakahara et al., 2012), which is converted to hexadecanal by Dpl1 in the endoplasmic reticulum (Kihara, 2014) (Figure S3A). Q levels were normal in Δ*dpl1* cells (Figure S3B), indicating that dihydrosphingosine degradation is independent from Q biosynthesis. Because of its aldehyde dehydrogenase activity and its partial localization at the mitochondrial outer membrane (Zahedi et al., 2006), we hypothesized that Hfd1 might catalyze the dehydrogenation of 4-Hbz to form 4-HB for mitochondrial Q biosynthesis (Figure S3C). 4-Hbz efficiently increased Q in WT but not in Δ*hfd1* cells (Figure 3A), showing that the use of 4-Hbz as a precursor of Q requires Hfd1. Dehydrogenation of 4-Hbz or decanal was diminished in cellular extracts from Δ*hfd1* cells and was increased in Δ*hfd1+HFD1* (Figures S3D and S3E). The 4-Hbz dehydrogenase activity was mainly associated with the membrane fraction (Figure S3F) and mitochondria from WT or Δ*hfd1+HFD1* cells showed a robust oxidation of 4-Hbz into 4-HB, unlike those from Δ*hfd1* cells (Figure 3B). We further verified the capacity of Hfd1 to synthesize 4-HB from 4-Hbz in a heterologous system, the *E. coli* Δ*ubiC* strain, which is impaired in 4-HB biosynthesis (Siebert et al., 1994). Addition of 4-HB complemented the Q deficiency of the *E. coli* Δ*ubiC* strain (Figure 3C), whereas efficient complementation by 4-Hbz required the expression of a functional Hfd1 protein (Figure 3C). Finally, we purified Hfd1 fused to the maltose binding protein (Figure S3G). MBP-Hfd1 oxidized benzaldehyde and 4-Hbz (Figure 3D), and preferred

NAD to NADP as a co-substrate (Figure S3H). Collectively, these data demonstrate that Hfd1 oxidizes 4-Hbz to 4-HB to supply Q biosynthesis in mitochondria.

4-Hbz is the last intermediate in the Tyr to 4-HB pathway

Next, we quantified 4-Hbz in yeast cellular extracts and found an increase upon addition of tyrosine to the culture medium (Figure S3I). $^{15}N^{13}C_9$-tyrosine yielded a +7 m/z increment in 4-Hbz, demonstrating that all carbon atoms of 4-Hbz were labelled (Figure S3J). The labelling of the 4-Hbz pool was comparable in WT and Δ*hfd1* cells but decreased in Δ*aro8*Δ*aro9* cells (Figure 3E). Together, these results establish that 4-Hbz is located downstream of 4-HPP in the pathway that converts tyrosine into 4-HB.

Human ALDH3A1 oxidizes 4-Hbz to 4-HB in *S. cerevisiae*

Humans possess 19 aldehyde dehydrogenases (Jackson et al., 2011) and a phylogenetic analysis revealed that Hfd1 clustered with the four members of subfamily 3 (Figure S4). Since the defect of Δ*hfd1* cells in dihydrosphingosine degradation was complemented by human *ALDH3A2* and *ALDH3B1* (Kitamura et al., 2013), it was of interest to verify if any of the four members of subfamily 3 may oxidize 4-Hbz to 4-HB. All four proteins were expressed at similar levels in yeast Δ*hfd1* cells (Kitamura et al., 2013) (Figure 4A), but only extracts containing ALDH3A1 oxidized 4-Hbz *in vitro* (Figure 4A). ALDH3A1 increased Q levels in Δ*hfd1* cells when 4-Hbz was added to the culture medium (Figure 4B), showing the ability of ALDH3A1 to oxidize 4-Hbz to 4-HB *in vivo*.

DISCUSSION

Hfd1 fulfills two independent functions in sphingolipid and Q metabolisms

Our results demonstrate that Hfd1 is required for coenzyme Q biosynthesis by oxidizing 4-Hbz to 4-HB. Hfd1 was also shown to oxidize aliphatic aldehydes like hexadecanal, an intermediate in a degradation pathway of the sphingoid base dihydrosphingosine (Nakahara et al., 2012). We believe that the defects of Δ*hfd1* cells in sphingolipid and Q metabolisms are independent. Indeed, Δ*dpl1* cells which cannot degrade dihydrosphingosine (Nakahara et al., 2012) have a normal Q content (Figure S3B), showing that a disruption of the degradation pathway of dihydrosphingosine does not perturb Q biosynthesis. Furthermore, human ALDH3A2 and ALDH3B1 complemented the hexadecenal dehydrogenase defect of Δ*hfd1* cells (Kitamura et al., 2013) but did not restore Q biosynthesis (Figure 4B), whereas ALDH3A1

complemented the Q defect (Figure 4B) but not the dihydrosphingosine degradation defect (Kitamura et al., 2013), demonstrating the independence of both cellular processes. Human ALDH3A1 and ALDH3A2 may have evolved restricted substrate specificities compared to Hfd1 which combines dehydrogenase activities on aliphatic aldehydes like hexadecenal and aromatic aldehydes like 4-Hbz. Hfd1 is dually localized in the endoplasmic reticulum and in mitochondria (Zahedi et al., 2006) and each pool may specifically contribute to a particular metabolism since hexadecanal is synthesized by Dpl1 in the ER whereas Q biosynthesis occurs in mitochondria (Ikeda et al., 2004; Tran and Clarke, 2007)(Figure 5).

The supply of aromatic precursors for Q biosynthesis in *S. cerevisiae*

S. cerevisiae utilises 4-HB and pABA as aromatic precursors of Q (Marbois et al., 2010; Pierrel et al., 2010), yet their endogenous levels are limiting for Q biosynthesis since addition of either molecule to pABA-depleted growth medium increased the Q content of WT cells (Pierrel et al., 2010). Thus, the use of pABA-depleted medium was a prerequisite for the success of our forward genetic approach which revealed the requirement of Hfd1 for Q biosynthesis. Inactivation of *hfd1* diminished the influx of 4-HB but not pABA into Q biosynthesis (Figure 2E), but the endogenous pABA pool was insufficient to compensate the shortage of 4-HB since we showed that Δ*hfd1* cells were profoundly deficient in Q (Figure 3A). Endogenous pABA may thus be predominantly used for folate biosynthesis (Figure S1A). We observed a partial restoration of Q levels in Δ*hfd1* cells overexpressing *COQ2-MVD1* (Figure 2C). Therefore, we think that endogenous pools of pABA and 4-HB may be more efficiently redirected towards Q biosynthesis upon overexpression of the 4-HB/pABA polyprenyltransferase Coq2. Altogether, we conclude that WT cells use 4-HB as the main precursor of Q under our growth conditions and that 4-HB is synthesized from the shikimate pathway and from exogenous tyrosine via a common intermediate, 4-HPP (Figure 5). Inactivation of either branch of 4-HPP synthesis maintained, and even increased Q levels in the case of Δ*tyr1* cells (Figure 1), reflecting compensatory mechanisms that might be linked to the extensive regulation of the shikimate pathway (Braus, 1991).

The pathway from tyrosine to 4-HB and its potential conservation in higher eukaryotes

Altogether, our results reveal several steps of the metabolic pathway from tyrosine to 4-HB and establish 4-HPP and 4-Hbz as the first and last intermediates, respectively. How the side chain of 4-HPP is shortened remains to be elucidated. However, contrary to what was previously hypothesized (Clarke, 2000; Turunen et al., 2004), β-oxidation is probably not

involved, since it would form directly 4-HB but not 4-Hbz (Figure 5) (Widhalm and Dudareva, 2015), whereas we have demonstrated that Q biosynthesis requires the oxidation of 4-Hbz by Hfd1. The hydration of 4-coumaric acid and a subsequent retro-aldol reaction to yield 4-Hbz is a more likely scenario for the shortening of the side chain (Clarke, 2000) (Figure 5) since *S. cerevisiae* was recently shown to incorporate 4-coumaric acid into Q, although not efficiently (Xie et al., 2015).

About half of 4-HB used for Q biosynthesis in the plant *A. thaliana* originates from tyrosine through an unknown metabolic pathway (Block et al., 2014). The final reaction may be the oxidation of 4-Hbz since aromatic aldehyde dehydrogenase activities with broad substrate specificities were reported in developing seeds of *A. thaliana* and in hairy roots of *Daucus carota* (Ibdah et al., 2009; Sircar et al., 2011). Tyrosine also supports Q biosynthesis in animals (Olson, 1966) and it will be important to verify whether mammalian 4-HB biosynthesis shares similarities with the yeast pathway. Tyrosine aminotransferase (TAT) catalyzes the deamination of tyrosine in the liver and is mutated in tyrosinemia type II (Dietrich, 1992; Scott, 2006). Measurements of Q levels in patients will indicate if TAT is required for Q biosynthesis. Animals may also rely on the oxidation of 4-Hbz to generate 4-HB because radiolabelled 4-Hbz was incorporated into Q when injected to rats (Ranganathan and Ramasarma, 1975) and when added to rat kidneys *in vitro* (Parson and Rudney, 1964). Since a deficit in 4-HB biosynthesis is expected to cause Q deficiency, our work calls for patients with genetically unassigned Q deficiency to be screened for mutations in aldehyde dehydrogenase genes, especially *ALDH3A1*.

SIGNIFICANCE

Coenzyme Q is a redox lipid that is central for energetic metabolism of eukaryotes. The biosynthesis of Q from the aromatic precursor 4-hydroxybenzoic acid (4-HB) is conserved and requires multiple catalytic reactions and associated proteins. Mutations in corresponding genes cause primary coenzyme Q deficiencies and result in various severe human diseases which are often improved by coenzyme Q supplementation. However, the hydrophobicity of coenzyme Q and therefore its poor bioavailability is thought to limit the efficiency of the treatment. In eukaryotes, biosynthesis of 4-HB from tyrosine has been suspected for forty years, yet, the pathway from tyrosine to 4-HB has remained elusive to date. We partially solved the long-standing problem of the biosynthesis of the aromatic precursor of coenzyme Q by providing a molecular understanding of the first and last reactions of the pathway in the yeast *S. cerevisiae*, namely the deamination of tyrosine to 4-hydroxyphenylpyruvate by Aro8 and Aro9 and the

oxidation of 4-hydroxybenzaldehyde to 4-HB by Hfd1. Whereas part of 4-HB is also provided by the shikimate pathway in *S. cerevisiae,* the importance of the tyrosine to 4-HB pathway for Q biosynthesis is likely to be more preponderant in higher eukaryotes which lack the shikimate pathway. We found that inactivation of *hfd1* resulted in coenzyme Q deficiency which was efficiently complemented by the addition of exogenous 4-HB. Our demonstration that human ALDH3A1 is able to oxidize 4-hydroxybenzaldehyde to 4-HB represent the first stage in assessing the conservation of the tyrosine to 4-HB pathway from yeast to humans. Mutations in genes of the tyrosine to 4-HB pathway may lead to coenzyme Q deficiencies in humans. In such cases, Q levels might be restored in patients by supplementation with 4-HB, a hydrophilic compound that might prove more bioavailable than exogenous Q which is normally used to treat coenzyme Q deficiencies.

EXPERIMENTAL PROCEDURES

Plasmids and strains. Plasmids and strains used in this study are detailed in Supplemental Information.

Yeast culture conditions. Yeast strains were grown at 30 °C and 200 rpm shaking in YPD (1% (w/v) yeast extract, 2% (w/v) peptone and 2% (w/v) glucose) or in YNB-p (YNB without pABA and without folate, MP Biomedicals) supplemented with 10 mg/L folate, 10 µM $FeCl_3$, 2% (w/v) carbon source (glucose, galactose or lactate-glycerol (LG)) and nutrients to cover the strains auxotrophies in quantities described in (Sherman, 2002). We note that exogenously added folate is unlikely to be imported in yeast (Nguyen and Clarke, 2012). When necessary, aromatic amino acids were added at a final concentration of 20 mg/L for tryptophane, 50 mg/L for phenylalanine and 15-60 mg/L for tyrosine as indicated (Sherman, 2002). For labelling experiments, 30 mg/L $^{15}N^{13}C_9$-tyrosine or 50 mg/L $^{13}C_9$-phenylalanine were added in replacement of the unlabelled amino acid. Only L-isomers of amino acids were used. YNB-p 2% galactose liquid cultures were performed by inoculating fresh medium with an aliquot of a 24 h culture grown in YNB-p 2% galactose 0.2% glucose. Bacto-agar (Euromedex) was added at 1.6% (w/v) for solid media.

Analysis of coenzyme Q content. Yeast cells were grown to OD_{600} = 1 in YNB-p galactose medium unless otherwise stated and cooled down on ice prior to collection by centrifugation and determination of the cells wet weight (Ozeir et al., 2015). Lipid extraction and Q analysis by HPLC-electrochemical detection (ECD) including MS detection or not was performed as previously described (Ozeir et al., 2015). Total Q was calculated from the ECD signal, unlabelled-Q and labelled $^{13}C_6$-Q were quantified by integrating the peaks obtained at the

retention time of Q for the positive ions m/z 591.2 and 597.2, respectively. *E. coli* cells grown overnight in M9 medium containing 100 µg/mL ampicillin for plasmid selection as needed, were inoculated at OD_{600} = 0.05 in M9 medium containing 30 µM isopropyl β-D-1-thiogalactopyranoside (IPTG) and supplemented or not with 4-HB or 4-Hbz. Cells were grown at 37 °C, 200 rpm shaking until OD_{600} = 0.8 and analyzed for Q content by HPLC-ECD as previously described (Aussel et al., 2014).

4-Hbz dehydrogenase activity assays. For yeast extract activity assays, cell pellets (10 mL of yeast culture collected at OD_{600} = 1) were resuspended in 1 mL PIPES 100 mM pH 7.1 with 2 pellet-volumes of glass beads and vortexed during 10 min. Cell homogenates were pipetted to eliminate the glass beads and centrifuged at 15,000 rpm, 4 °C during 5 min; resulting supernatants, corresponding to soluble fractions were collected, and pellets, corresponding to membrane fractions were resuspended in 500 µL PIPES 100 mM pH 7.1. Cell homogenates collected prior to centrifugation corresponded to total extracts. Protein content was measured by the BCA method. 20 µL of each fraction was assayed for 4-Hbz dehydrogenase activity by incubation at 30 °C for 1 h in a total volume of 100 µL PIPES 50 mM pH 7.1, 500 µM NAD^+, 100 µM 4-Hbz . Mitochondrial fractions (20 µL in PIPES 100 mM pH 7.1 mannitol 1.2 M, protein concentration ~1.5 µg/µL) were assayed similarly except that the assay buffer contained 0.6 M mannitol. The reaction was stopped by adding 2 µL pure formic acid. 4-HB and 4-Hbz were extracted as described elsewhere (Villas-Bôas et al., 2005). Briefly, 500 µL cold methanol was added to samples together with 10 µL of 10 µM vanillic acid (VA) used as an internal standard. The mixture was frozen in liquid nitrogen, stored if necessary at -80 °C, then thawed on ice and centrifuged at 770 g during 20 min at 4 °C. The supernatant was collected and evaporated under nitrogen at 60 °C. Samples were resuspended in water containing 0.25% (v/v) acetic acid and analyzed by HPLC (U3000 Dionex) on a NUCLEODUR® PFP column (Macherey-Nagel, 3 µm, 2 x 150 mm). Two mobile phases were used for elution at a flow rate of 0.25 mL/min: 0.25% (v/v) acetic acid in water (A) and methanol (B). The linear gradient profile was 0-2 min, 5% B; 2-12 min, 5-30% B; 12-18 min, 30% B; 18-20 min, 30-5% B; 20-24 min, 5% B. 4-HB, VA and 4-Hbz were detected by a diode array detector which recorded the absorbance at 260 nm (4-HB and VA) and 290 nm (4-Hbz). The recovery of VA was typically 75% and was used to correct 4-HB values for loss during extraction.

Mitochondrial preparation and Western blotting. Purification of mitochondria and immunodetection were conducted as described previously (Ozeir et al., 2015). Monoclonal anti-Flag M2 antibody (F1804, Sigma, dilution 1/3,000) and polyclonal anti-Anc2 antibody (dilution

1/1,500) were detected with HRP-coupled anti-mouse IgG and HRP-coupled protein A, respectively.

Extraction and GC-MS analysis of 4-Hbz. Cells were cultured until OD_{600} ~ 2 in 50 mL YNB-p galactose supplemented or not with aromatic amino acids and 30 mg/L $^{15}N^{13}C_9$-tyrosine, transferred into precooled 50 mL falcon tubes, and centrifuged for 1 min at 4,000 rpm, 4 °C. The cell pellet was resuspended in 10 mL ice cold PBS and centrifugation was repeated. The supernatant was eliminated and the cells were vortexed in 5 mL acetonitrile/methanol/water (2/2/1, v/v) precooled at -20 °C. The suspension was stored at -80 °C until further use. The suspension was then allowed to thaw at room temperature for 30 min and was centrifuged for 2 min at 4,000 rpm, 20 °C. The supernatant was transferred into a 50 mL falcon tube using Pasteur pipette and was supplemented with 5 mL water, 1% (v/v) acetic acid, 2 g NaCl, and 100 ng VA as an extraction standard. The mixture was homogenized by vortexing, 10 mL ethyl acetate was added and vortex was repeated. After phase separation, the upper ethyl acetate phase was taken and the extraction was repeated with 10 mL ethyl acetate. The ethyl acetate phases were combined and dried in a water bath at 37 °C under a stream of nitrogen. The sample was dissolved in 1.2 mL ethanol and centrifuged for 2 min at 13,000 rpm at room temperature. The resulting supernatant was transferred to Eppendorf tubes, dried under nitrogen and stored at -80 °C. On the day of the analysis, samples were dissolved in 50 µL of O-methoxyamine-HCl (20 mg/mL in pyridine) and incubated at 60 °C for 30 min; 50 µL of BSTFA-TMCS (99:1, Macherey Nagel) was then added and samples were further incubated at 60 °C for 30 min. Samples were centrifuged at 13,000 rpm for 1 min. Derivatized samples were analysed by Gas Chromatography-Mass Spectrometry (GC-MS) using an Agilent 5973 Mass Selective Detector coupled to an HP6890 GC system equipped with an Optima-17-MS capillary column (30 m x 0.25 mm x 0.25 µm; Macherey-Nagel). The carrier gas was helium and the injection volume was 2.5 µl with an inlet temperature of 250 °C, with a split ratio of 50:1 for full scan detection and 20:1 for SIM, at an inlet temperature of 250 °C. The initial oven temperature was 75 °C for 3 min, then increased to 250 °C at a rate of 12 °C/min, held for 1 min then increased to 300 °C at 10 °C/min and held for 5 min. The MSD transfer line heater, MS source and MS quad temperatures were set at 280 °C, 230 °C and 150 °C, respectively. The mass range used for full scan detection of 4-Hbz was m/z 204-234 with an abundance threshold set at 150. The mass ions and windows used for SIM were as follows: 4Hbz, 208 (M^+-CH_3), 215 ($^{13}C_7M^+$-CH_3), 223 (M^+), 230 ($^{13}C_7M^+$) from 5 to 12 min; VA, 223 (M^+-CH_3-TMS-H), 253 (M^+-$Si(CH_3)_2$-H), 267 (M^+-$(CH_3)_3$) and 297 (M^+-CH_3) from 12 min to 15 min. Standards containing 20 ng VA and 4-Hbz were analyzed in similar conditions and used for quantification. Sample loss during

extraction was corrected by calculating the recovery of VA in the different samples (typically 80-95%) and quantities of 4-Hbz were normalized to OD values of the harvested cells. Labelling of 4-Hbz was calculated by averaging the ratios of the abundance of the unlabelled/labelled ion pairs 208/215 and 223/230.

Bioinformatics methods. Sequence alignments were generated with Clustal Omega (http://www.ebi.ac.uk/Tools/msa/clustalo/). The homology model of Hfd1 was constructed with Phyre2 (Kelley et al., 2015) used in intensive mode. The program selected the aldehyde dehydrogenase 3A1 from *Rattus norvegicus* (PDB code 1AD3) as template. For the phylogenetic analysis, the protein sequences were retrived from NCBI and were aligned using the MUSCLE software (http://www.ebi.ac.uk/Tools/msa/muscle/). The resulting sequence alignment file was then processed with the latest version of the PHYLIP package (http://evolution.genetics.washington.edu/phylip), which comprises the PROTDIST program to compute a matrix distance and the DRAWGRAM program to plot the phylogenetic tree constructed with the Neighbor-Joining method.

Statistical methods. Results are presented as mean ± s.e.m. Data sets were compared by unpaired two-tailed *t*-test or an analysis of variance (ANOVA) using GraphPad Prism 6 software.

SUPPLEMENTAL INFORMATION

Supplemental Information includes Supplemental Experimental Procedures and four figures.

AUTHOR CONTRIBUTIONS

L.-A.P., M.L, L.P., J.C.W. and F.P. designed research, performed experiments, analyzed and interpreted the data; A.K. contributed reagents; F.P. supervised the project and wrote the manuscript; all authors discussed the results and commented on the manuscript.

ACKNOWLEDGMENTS

We thank Laurent Loiseau for constructing the pBADKI-*UBIC* vector, Dr Joël Gaffé for assistance with the phylogenetic analysis, Dr Pavel Sindelar, Dr Vassilis Vassiliou and Ulrika Forsman for discussions. This work was supported by the Fondation pour la Recherche Médicale (FRM), grant number «DPM20121125553» to F. Pierrel.

REFERENCES

Ashby, M.N., Kutsunai, S.Y., Ackerman, S., Tzagoloff, A., and Edwards, P.A. (1992). *COQ2* is a candidate for the structural gene encoding para-hydroxybenzoate:polyprenyltransferase. J. Biol. Chem. *267*, 4128-4136.

Aussel, L., Loiseau, L., Hajj Chehade, M., Pocachard, B., Fontecave, M., Pierrel, F., and Barras, F. (2014). ubiJ, a New Gene Required for Aerobic Growth and Proliferation in Macrophage, Is Involved in Coenzyme Q Biosynthesis in Escherichia coli and Salmonella enterica Serovar Typhimurium. J. Bacteriol. *196*, 70-79.

Bentinger, M., Tekle, M., and Dallner, G. (2010). Coenzyme Q-biosynthesis and functions. Biochem. Biophys. Res. Commun. *396*, 74-79.

Bentley, R. (1990). The shikimate pathway--a metabolic tree with many branches. Crit. Rev. Biochem. Mol. Biol. *25*, 307-384.

Block, A., Widhalm, J.R., Fatihi, A., Cahoon, R.E., Wamboldt, Y., Elowsky, C., Mackenzie, S.A., Cahoon, E.B., Chapple, C., Dudareva, N., *et al.* (2014). The Origin and Biosynthesis of the Benzenoid Moiety of Ubiquinone (Coenzyme Q) in Arabidopsis. Plant Cell *26*, 1938-1948.

Botet, J., Mateos, L., Revuelta, J.L., and Santos, M.A. (2007). A chemogenomic screening of sulfanilamide-hypersensitive Saccharomyces cerevisiae mutants uncovers ABZ2, the gene encoding a fungal aminodeoxychorismate lyase. Eukaryot Cell *6*, 2102-2111.

Braus, G.H. (1991). Aromatic amino-acid biosynthesis in the yeast Saccharomyces cerevisiae: a model system for the regulation of a eukaryotic biosynthetic pathway. Microbiological Reviews *55*, 349-370.

Clarke, C.F. (2000). New advances in coenzyme Q biosynthesis. Protoplasma *213*, 134-147.

Cluis, C.P., Ekins, A., Narcross, L., Jiang, H., Gold, N.D., Burja, A.M., and Martin, V.J. (2011). Identification of bottlenecks in Escherichia coli engineered for the production of CoQ(10). Metab. Eng., in press.

Dietrich, J.B. (1992). Tyrosine aminotransferase: a transaminase among others. Cell. Mol. Biol. *38*, 95-114.

Forsgren, M., Attersand, A., Lake, S., Grunler, J., Swiezewska, E., Dallner, G., and Climent, I. (2004). Isolation and functional expression of human COQ2, a gene encoding a polyprenyl transferase involved in the synthesis of CoQ. Biochem. J. *382*, 519-526.

Freyer, C., Stranneheim, H., Naess, K., Mourier, A., Felser, A., Maffezzini, C., Lesko, N., Bruhn, H., Engvall, M., Wibom, R., *et al.* (2015). Rescue of primary ubiquinone deficiency due to a novel COQ7 defect using 2,4-dihydroxybensoic acid. J Med Genet.

Genova, M.L., and Lenaz, G. (2014). Functional role of mitochondrial respiratory supercomplexes. Biochim. Biophys. Acta *1837*, 427-443.

Gonzalez-Mariscal, I., Garcia-Teston, E., Padilla, S., Martin-Montalvo, A., Pomares-Viciana, T., Vazquez-Fonseca, L., Gandolfo-Dominguez, P., and Santos-Ocana, C. (2014). Regulation of coenzyme Q biosynthesis in yeast: A new complex in the block. IUBMB Life *66*, 63-70.

Ibdah, M., Chen, Y.T., Wilkerson, C.G., and Pichersky, E. (2009). An Aldehyde Oxidase in Developing Seeds of Arabidopsis Converts Benzaldehyde to Benzoic Acid. Plant Physiol. *150*, 416-423.

Ikeda, M., Kihara, A., and Igarashi, Y. (2004). Sphingosine-1-phosphate lyase SPL is an endoplasmic reticulum-resident, integral membrane protein with the pyridoxal 5 '-phosphate binding domain exposed to the cytosol. Biochem. Biophys. Res. Commun. *325*, 338-343.

Jackson, B., Brocker, C., Thompson, D.C., Black, W., Vasiliou, K., Nebert, D.W., and Vasiliou, V. (2011). Update on the aldehyde dehydrogenase gene (ALDH) superfamily. Human genomics *5*, 283-303.

Johnson, A., Gin, P., Marbois, B.N., Hsieh, E.J., Wu, M., Barros, M.H., Clarke, C.F., and Tzagoloff, A. (2005). *COQ9*, a new gene required for the biosynthesis of coenzyme Q in *Saccharomyces cerevisiae*. J. Biol. Chem. *280*, 31397-31404.
Kawamukai, M. (2016). Biosynthesis of coenzyme Q in eukaryotes. Bioscience Biotechnology and Biochemistry *80*, 23-33.
Kelley, L.A., Mezulis, S., Yates, C.M., Wass, M.N., and Sternberg, M.J. (2015). The Phyre2 web portal for protein modeling, prediction and analysis. Nat. Protoc. *10*, 845-858.
Kihara, A. (2014). Sphingosine 1-phosphate is a key metabolite linking sphingolipids to glycerophospholipids. Biochim. Biophys. Acta *1841*, 766-772.
Kitamura, T., Naganuma, T., Abe, K., Nakahara, K., Ohno, Y., and Kihara, A. (2013). Substrate specificity, plasma membrane localization, and lipid modification of the aldehyde dehydrogenase ALDH3B1. Biochim. Biophys. Acta *1831*, 1395-1401.
Lang, B.S., Gorren, A.C., Oberdorfer, G., Wenzl, M.V., Furdui, C.M., Poole, L.B., Mayer, B., and Gruber, K. (2012). Vascular bioactivation of nitroglycerin by aldehyde dehydrogenase-2: reaction intermediates revealed by crystallography and mass spectrometry. J. Biol. Chem. *287*, 38124-38134.
Laredj, L.N., Licitra, F., and Puccio, H.M. (2014). The molecular genetics of coenzyme Q biosynthesis in health and disease. Biochimie *100*, 78-87.
Lu, W., Ye, L., Lv, X., Xie, W., Gu, J., Chen, Z., Zhu, Y., Li, A., and Yu, H. (2015). Identification and elimination of metabolic bottlenecks in the quinone modification pathway for enhanced coenzyme Q production in Rhodobacter sphaeroides. Metab. Eng.
Marbois, B., Xie, L.X., Choi, S., Hirano, K., Hyman, K., and Clarke, C.F. (2010). para-aminobenzoic acid is a precursor in coenzyme Q(6) biosynthesis in *Saccharomyces cerevisiae*. J. Biol. Chem. *285*, 27827-27838.
Moriyama, D., Hosono, K., Fujii, M., Washida, M., Nanba, H., Kaino, T., and Kawamukai, M. (2015). Production of CoQ10 in fission yeast by expression of genes responsible for CoQ10 biosynthesis. Biosci. Biotechnol. Biochem. *79*, 1026-1033.
Nakahara, K., Ohkuni, A., Kitamura, T., Abe, K., Naganuma, T., Ohno, Y., Zoeller, R.A., and Kihara, A. (2012). The Sjogren-Larsson syndrome gene encodes a hexadecenal dehydrogenase of the sphingosine 1-phosphate degradation pathway. Mol. Cell *46*, 461-471.
Nguyen, T.P., and Clarke, C.F. (2012). Folate status of gut microbiome affects Caenorhabditis elegans lifespan. BMC Biol *10*, 66.
Olson, R.E. (1966). Biosynthesis of ubiquinones in animals. Vitam Horm *24*, 551-574.
Olson, R.E., Dialameh, G.H., Bentley, R., Springer, C.M., and Ramsey, V.G. (1965). Studies on coenzyme Q - Pattern of labeling in coenzyme Q9 after adminstration of isotopic acetate and aromatic amino acids to rats. J. Biol. Chem. *240*, 514-&.
Olson, R.E., and Rudney, H. (1983). Biosynthesis of ubiquinone. Vitam. Horm. *40*, 1-43.
Ozeir, M., Muhlenhoff, U., Webert, H., Lill, R., Fontecave, M., and Pierrel, F. (2011). Coenzyme Q biosynthesis: Coq6 Is required for the C5-hydroxylation reaction and substrate analogs rescue Coq6 deficiency. Chem. Biol. *18*, 1134-1142.
Ozeir, M., Pelosi, L., Ismail, A., Mellot-Draznieks, C., Fontecave, M., and Pierrel, F. (2015). Coq6 Is Responsible for the C4-deamination Reaction in Coenzyme Q Biosynthesis in Saccharomyces cerevisiae. J. Biol. Chem. *290*, 24140-24151.
Parajuli, B., Fishel, M.L., and Hurley, T.D. (2014). Selective ALDH3A1 inhibition by benzimidazole analogues increase mafosfamide sensitivity in cancer cells. J. Med. Chem. *57*, 449-461.
Parson, W.W., and Rudney, H. (1964). Biosynthesis of benzoquinone ring of ubiquinone from p-hydroxybenzaldehyde + p-hydroxybenzoic acid in rat kidney azotobacter vinelandii + bakers yeast. Proc. Natl. Acad. Sci. U. S. A. *51*, 444-450.

Pierrel, F., Hamelin, O., Douki, T., Kieffer-Jaquinod, S., Muhlenhoff, U., Ozeir, M., Lill, R., and Fontecave, M. (2010). Involvement of mitochondrial ferredoxin and para-aminobenzoic acid in yeast coenzyme Q biosynthesis. Chem. Biol. *17*, 449-459.
Quinzii, C.M., and Hirano, M. (2011). Primary and secondary CoQ(10) deficiencies in humans. BioFactors *37*, 361-365.
Ranganathan, S., and Ramasarma, T. (1975). Regulation of biosynthesis of ubiquinone in rat. Biochem. J. *148*, 35-39.
Salviati, L., Trevisson, E., Rodriguez Hernandez, M.A., Casarin, A., Pertegato, V., Doimo, M., Cassina, M., Agosto, C., Desbats, M.A., Sartori, G., *et al.* (2012). Haploinsufficiency of *COQ4* causes coenzyme Q_{10} deficiency. J Med Genet *49*, 187-191.
Scott, C.R. (2006). The genetic tyrosinemias. Am J Med Genet C Semin Med Genet *142C*, 121-126.
Sherman, F. (2002). Getting started with yeast. Methods Enzymol. *350*, 3-41.
Siebert, M., Severin, K., and Heide, L. (1994). Formation of 4-hydroxybenzoate in Escherichia coli: characterization of the ubiC gene and its encoded enzyme chorismate pyruvate-lyase. Microbiology *140 (Pt 4)*, 897-904.
Sircar, D., Mukherjee, C., Beuerle, T., Beerhues, L., and Mitra, A. (2011). Characterization of p-hydroxybenzaldehyde dehydrogenase, the final enzyme of p-hydroxybenzoic acid biosynthesis in hairy roots of Daucus carota. Acta Physiologiae Plantarum *33*, 2019-2024.
Tran, U.C., and Clarke, C.F. (2007). Endogenous synthesis of coenzyme Q in eukaryotes. Mitochondrion *7*, S62-71.
Turunen, M., Olsson, J., and Dallner, G. (2004). Metabolism and function of coenzyme Q. Biochim. Biophys. Acta *1660*, 171-199.
Urrestarazu, A., Vissers, S., Iraqui, I., and Grenson, M. (1998). Phenylalanine- and tyrosine-auxotrophic mutants of Saccharomyces cerevisiae impaired in transamination. Mol Gen Genet *257*, 230-237.
Villas-Bôas, S.G., Højer-Pedersen, J., Akesson, M., Smedsgaard, J., and Nielsen, J. (2005). Global metabolite analysis of yeast: evaluation of sample preparation methods. Yeast *22*, 1155-1169.
Wang, Y., and Hekimi, S. (2012). Molecular genetics of ubiquinone biosynthesis in animals. Crit. Rev. Biochem. Mol. Biol.
Wang, Y., and Hekimi, S. (2016). Understanding Ubiquinone. Trends in Cell Biology *26*, 367-378.
Widhalm, J.R., and Dudareva, N. (2015). A Familiar Ring to It: Biosynthesis of Plant Benzoic Acids. Molecular Plant *8*, 83-97.
Xie, L.X., Ozeir, M., Tang, J.Y., Chen, J.Y., Kieffer-Jaquinod, S., Fontecave, M., Clarke, C.F., and Pierrel, F. (2012). Over-expression of the Coq8 kinase in Saccharomyces cerevisiae coq null mutants allows for accumulation of diagnostic intermediates of the Coenzyme Q6 biosynthetic pathway. J. Biol. Chem. *287*, 23571-23581.
Xie, L.X., Williams, K.J., He, C.H., Weng, E., Khong, S., Rose, T.E., Kwon, O., Bensinger, S.J., Marbois, B.N., and Clarke, C.F. (2015). Resveratrol and para-coumarate serve as ring precursors for coenzyme Q biosynthesis. J. Lipid Res. *56*, 909-919.
Xu, W., Yuan, J., Yang, S., Ching, C.B., and Liu, J. (2016). Programming Saposin-Mediated Compensatory Metabolic Sinks for Enhanced Ubiquinone Production. ACS Synth Biol.
Zahedi, R.P., Sickmann, A., Boehm, A.M., Winkler, C., Zufall, N., Schonfisch, B., Guiard, B., Pfanner, N., and Meisinger, C. (2006). Proteomic analysis of the yeast mitochondrial outer membrane reveals accumulation of a subclass of preproteins. Mol. Biol. Cell *17*, 1436-1450.
Zhou, L., Wang, J.Y., Wang, J.H., Poplawsky, A., Lin, S.J., Zhu, B.S., Chang, C.Q., Zhou, T.L., Zhang, L.H., and He, Y.W. (2013). The diffusible factor synthase XanB2 is a

bifunctional chorismatase that links the shikimate pathway to ubiquinone and xanthomonadins biosynthetic pathways. Mol. Microbiol. *87*, 80-93.

FIGURE LEGENDS

Figure 1: A genetic defect in the metabolism of tyrosine decreases Q.
A, Quantification of $^{13}C_6$-Q and unlabelled Q in cells grown with $^{15}N^{13}C_9$-Tyr or $^{13}C_9$-Phe. *n*=3 (Δ*aro8*Δ*aro9*), *n*=4 (WT, Δ*aro2* and Δ*tyr1*). Mean + s.e.m. of total Q (upper error bar), mean - s.e.m. of $^{13}C_6$-Q (lower error bar). The average percentage of $^{13}C_6$-Q is indicated on top of each bar, *P* value in comparison to WT + $^{15}N^{13}C_9$-Tyr. **B**, Q content of cells grown in medium with aromatic amino acids. Mean ± s.e.m.; *n*=6. **C**, Q content of cells grown in glucose medium with aromatic amino acids (Tyr 15 mg/L) supplemented with 10 µM 4-HB or 60 mg/L tyrosine. Mean ± s.e.m.; *n*=2 (+ Tyr), *n*=3 (± 4-HB). **D**, Growth of strains containing the indicated YEp352 plasmids on medium without aromatic amino acids (– Aro) or with Phe, Trp and 15 mg/L Tyr, containing either glucose (Glu) or lactate-glycerol (LG) and supplemented or not with 10 µM 4-HB. Representative images from one of three independent experiments are shown. ns: no significant difference, *: $P< 0.05$, **: $P<0.01$, ***: $P<0.001$, ****: $P<0.0001$, unpaired two-tailed *t* test (**A**, **B**), One-way ANOVA test (**C**). *n*, number of independent experiments.

Figure 2: Cells lacking *HFD1* are deficient in Q biosynthesis.
A, Growth of WT and Δ*hfd1* strains containing the indicated pRS415 plasmids on medium without aromatic amino acids containing either glucose (Glu) or lactate-glycerol (LG) supplemented or not with 10 µM 4-HB. Representative images from one of three independent experiments are shown. **B**, Q content of cells containing an empty vector (-), pRS415-*HFD1*, pRS415-*HFD1-S241L*, or pRS426-*UBIC* grown in medium supplemented or not with 10 µM 4-HB, 10 µM pABA, 30 mg/L Tyr or aromatic amino acids (Aro) as indicated. Mean ± s.e.m.; *n*=4 (except for Δ*hfd1* with pABA, *n*=3). **C**, Q content of Δ*hfd1* cells containing the indicated YEp352 plasmids and grown in medium supplemented with 15 mg/L Tyr. Mean ± s.e.m.; *n*=3. **D**, Quantification of $^{13}C_6$-Q and unlabelled Q in cells grown in medium containing 30 mg/L $^{15}N^{13}C_9$-Tyr (*n*=9). Mean + s.e.m. of total Q (upper error bar), mean - s.e.m. of $^{13}C_6$-Q (lower error bar). The average percentage of $^{13}C_6$-Q is indicated on top of each bar. **E**, Superimposition of HPLC-ECD chromatograms of lipid extracts of the indicated strains containing the p*COQ8* plasmid. Q_4, internal standard; 4-AP, 3-hexaprenyl-4-aminophenol and 4-HP, 3-hexaprenyl-4-hydroxyphenol (structures shown). Representative chromatograms from one of four independent experiments are shown. ns: no significant difference, *: $P< 0.05$, ****: $P<0.0001$, One-way ANOVA test (**B**), unpaired two-tailed *t* test (**C**). *n*, number of independent experiments.

Figure 3: Hfd1 oxidizes 4-Hbz to 4-HB that is used for Q biosynthesis.
A, Q content of cells grown in the presence or not of 10 µM 4-Hbz. Mean ± s.e.m.; *n*=4. **B**, 4-Hbz dehydrogenase activity measured on mitochondria purified from WT, Δ*hfd1* and Δ*hfd1* cells transformed with pRS415-*HFD1*. Mean ± s.e.m.; *n*=5. **C**, Q content of *E. coli* WT or Δ*ubiC* cells containing pMAL-c2-*HFD1* or pMAL-c2-*HFD1-S241L* grown in M9 medium supplemented or not with 10 µM 4-HB or 10 µM 4-Hbz. Mean ± s.e.m.; *n*=4. **D**, Dehydrogenase activity of MBP-Hfd1 with 4-Hbz or benzaldehyde (Bz). Mean ± s.e.m.; *n*=6 (4-Hbz), *n*=3 (Bz). **E,** Quantification of labelled and unlabelled 4-Hbz in cells grown in YNB-p galactose medium

containing Trp, Phe and 30 mg/L $^{15}N^{13}C_9$-Tyr (*n*=4). Mean + s.e.m. of total 4-Hbz (upper error bar), mean - s.e.m. of $^{13}C_7$-4-Hbz (lower error bar). The average percentage of $^{13}C_7$-4-Hbz is indicated on top of each bar, *P* value in comparison to WT. ns: no significant difference, *: *P*<0.05, ****: *P*<0.0001, unpaired two-tailed *t* test. *n*, number of independent experiments.

Figure 4: Human ALDH3A1 oxidizes 4-Hbz to 4-HB in *S. cerevisiae*.
A, 4-Hbz dehydrogenase activity measured on total cellular extracts of Δ*hfd1* cells transformed with YEp352 (-), pNK10 (3xFLAG-ALDH3A1), pNK5 (3xFLAG-ALDH3A2), pNK12 (3xFLAG-ALDH3AB1) or pNK14 (3xFLAG-ALDH3AB2). Mean ± s.e.m.; *n*=3. Immunodetection of ALDH3 proteins with anti-FLAG antibody; Anc2 was used as a loading control. **B**, Q content of Δ*hfd1* cells described in **4A**, grown in the presence or not of 10 μM 4-Hbz. Mean ± s.e.m.; *n*=3 . **: *P*<0.01, unpaired two-tailed *t* test. *n*, number of independent experiments.

Figure 5: Reactions catalyzed by Hfd1 in Q biosynthesis and in the dihydrosphingosine degradation pathway in *S. cerevisiae*.
Hfd1 and human ALDH3A2 catalyze the oxidation of hexadecanal to hexadecanoic acid (Nakahara et al., 2012), which is likely to take place in the endoplasmic reticulum (Kihara, 2014; Zahedi et al., 2006). In mitochondria, Hfd1 oxidizes 4-Hbz into 4-HB which is prenylated by Coq2 and further metabolized to Q (R, polyprenyl tail). 4-HPP originates both from exogenous tyrosine via Aro8 and Aro9 and from chorismic acid via Aro7 and Tyr1. The shortening of the side chain of 4-HPP may proceed via hydration of 4-coumaric acid and a subsequent retro-aldol reaction (grey arrows) but is unlikely to involve β-oxidation (dashed grey arrows) which would yield 4-HB and not 4-Hbz.

Figure 1

Click here to download Figure Fig1.tif

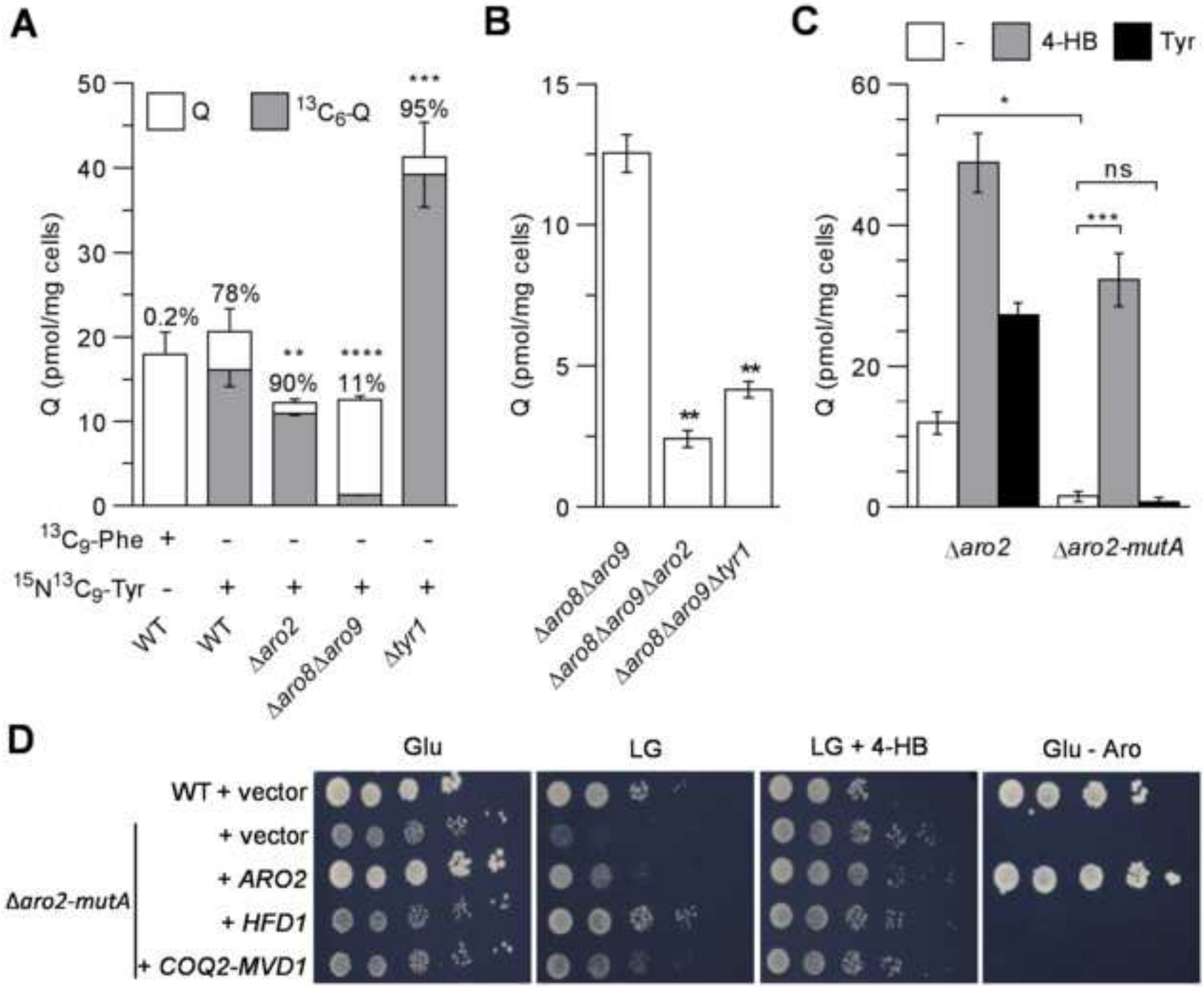

Figure 2

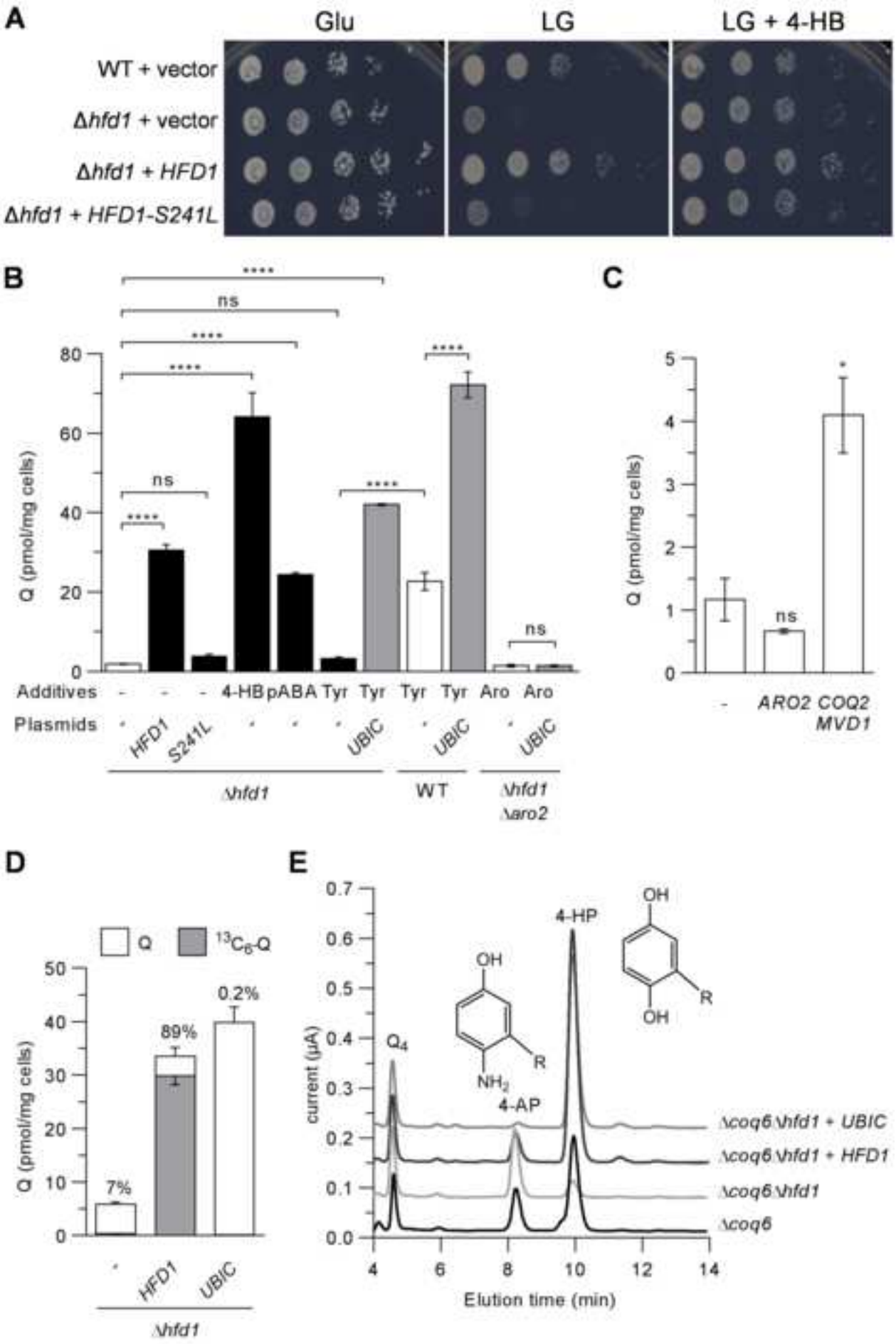

Figure 3

Click here to download Figure Fig3.tif

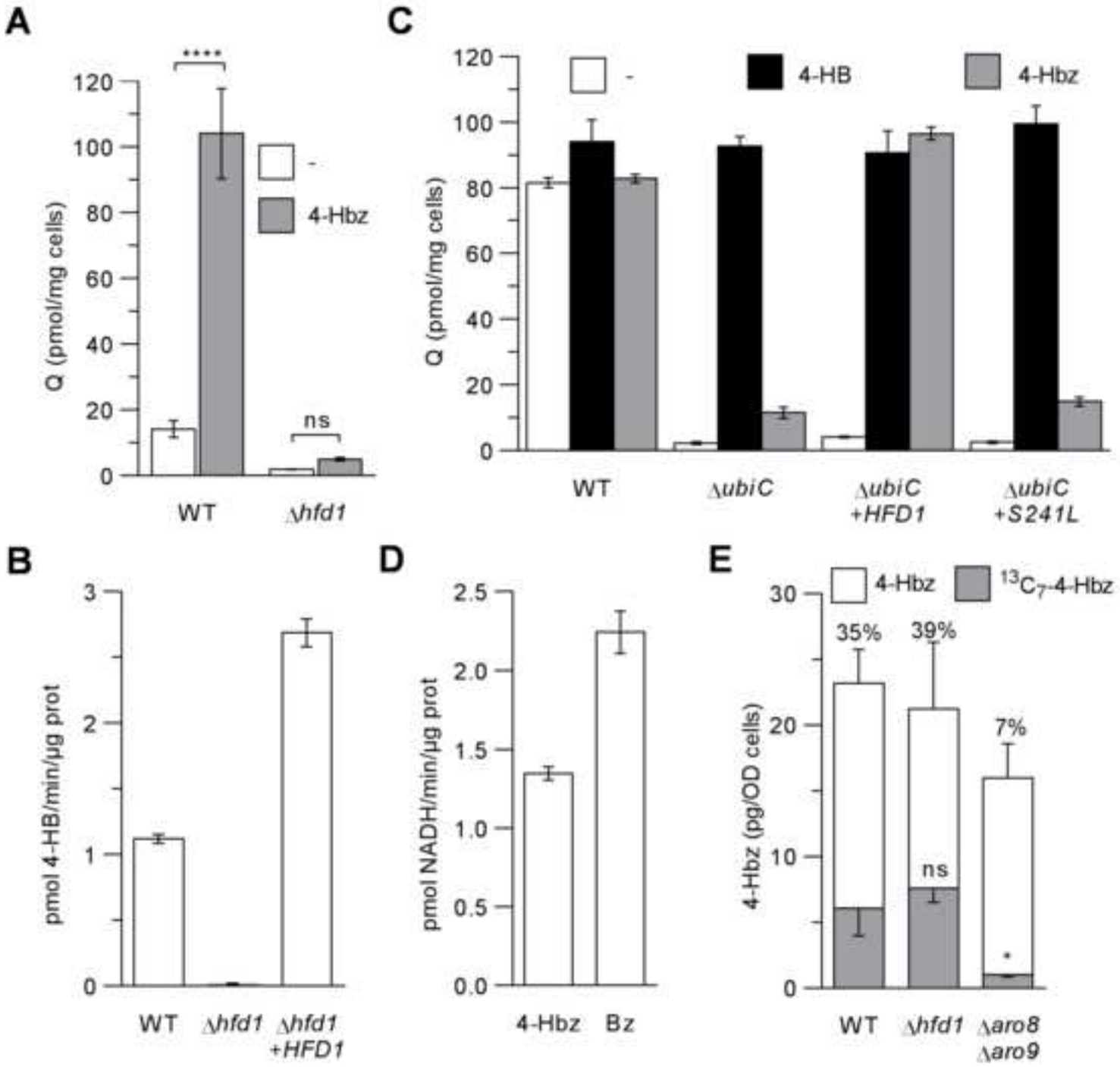

Figure 4

Click here to download Figure Fig4.tif

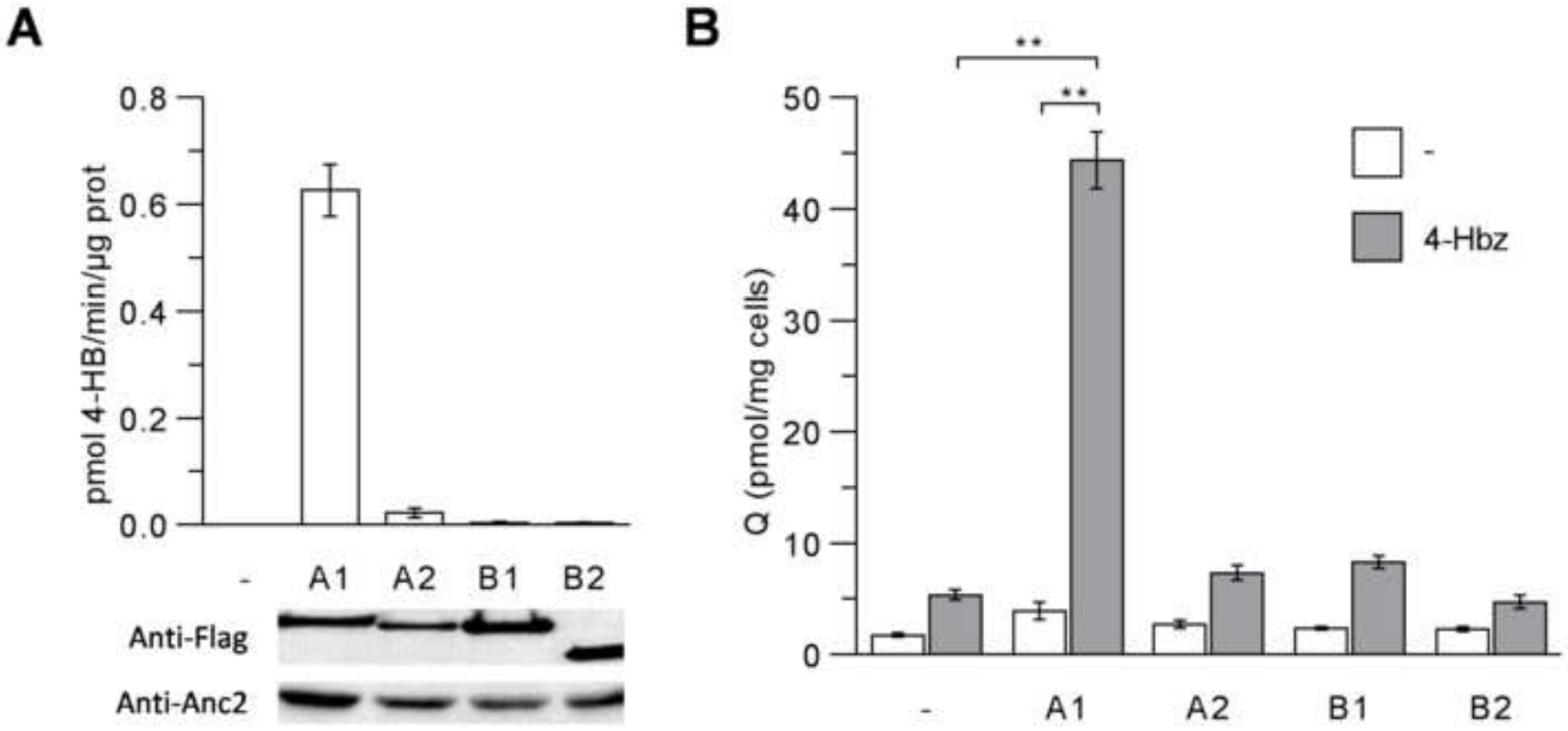

Figure 5

Click here to download Figure fig 5.tif

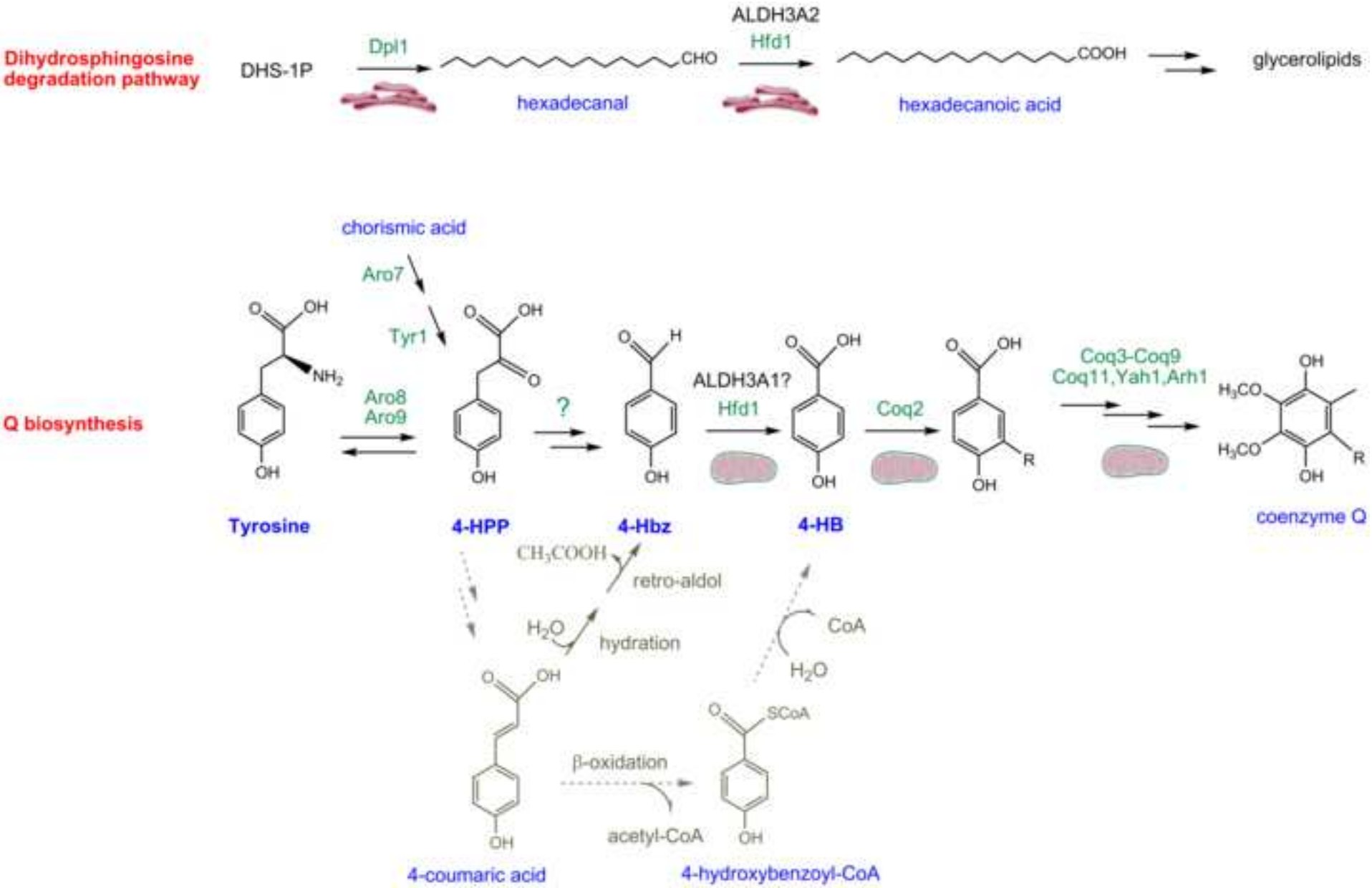

SUPPLEMENTAL INFORMATION

Figure S1

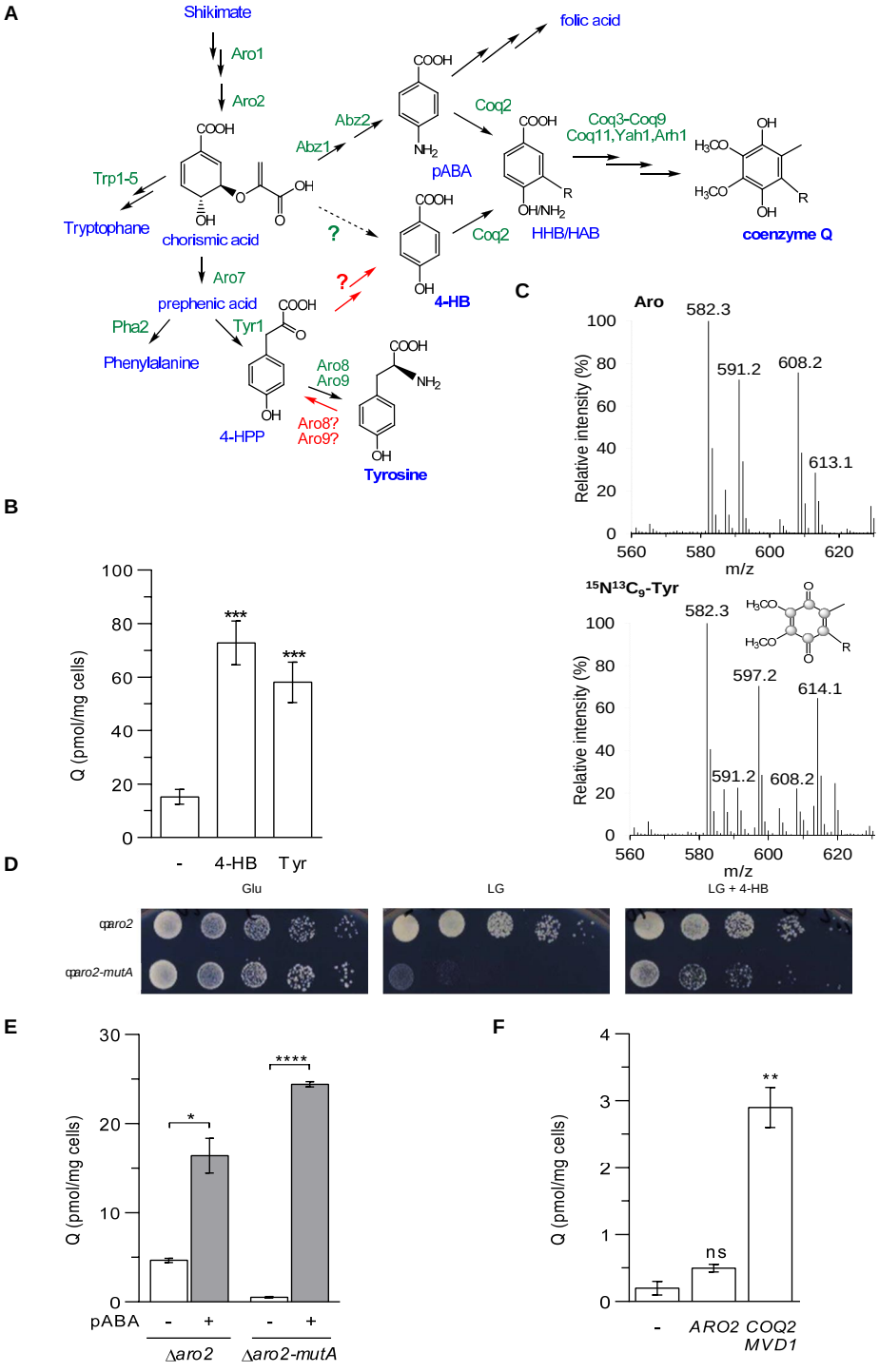

Figure S1 Related to Figure 1: Metabolic origin of the aromatic ring of coenzyme Q in *S. cerevisiae*.

A, The shikimate pathway and its proposed connections to coenzyme Q biosynthesis at the beginning of our study. 4-hydroxybenzoic acid (4-HB) and para-aminobenzoic acid (pABA) are prenylated by Coq2 to form hexaprenyl-hydroxybenzoic acid (HHB) and hexaprenyl-aminobenzoic acid (HAB), respectively. R represents the hexaprenyl tail of Q. Coq3-Coq9, Coq11, Yah1 and Arh1 are required to synthesize Q from HHB or HAB. The focus of this study is the biosynthesis of 4-HB which may originate either from tyrosine (red arrows) ï with 4-HPP as a hypothetical intermediate ï or from chorismic acid via a chorismatase reaction (dashed arrow) as catalysed by UbiC in *E. coli*. The metabolic pathway from tyrosine to 4-HB which takes into account the findings of our study is shown in Figure 5. **B**, Q content of WT cells grown in YNB-p galactose medium supplemented or not with 10 µM 4-HB or 60 mg/L tyrosine. Mean ± s.e.m.; *n*=8. **C**, Mass spectra of Q from WT cells grown in YNB-p galactose containing Phe, Trp and Tyr (Aro) or Phe, Trp and $^{15}N^{13}C_9$-Tyr. The ions at m/z= 591.2 and m/z= 608.2 correspond respectively to H^+- and NH_4^+-adducts of unlabeled Q ($C_{39}H_{58}O_4$); those at m/z= 597.2 and m/z= 614.1 correspond to H^+- and NH_4^+-adducts of ring-labeled Q ($^{13}C_6$-$^{12}C_{33}H_{58}O_4$). Grey dots indicate the positions of the ^{13}C isotope. The ion at m/z= 582.3 corresponds to an unidentified molecule which co-elutes with Q. Representative spectra from one of three independent experiments are shown. **D**, Plate growth assay of q*aro2* and q*aro2-mutA* strains on YNB-p solid medium with aromatic amino acids (Tyr 15 mg/L) containing either glucose (Glu) or lactate-glycerol (LG) supplemented or not with 10 µM 4-HB. Representative images from one of three independent experiments are shown. **E**, Q content of q*aro2* and q*aro2-mutA* cells grown in YNB-p galactose medium with aromatic amino acids (Tyr 15 mg/L) supplemented or not with 10 µM pABA. Mean ± s.e.m.; *n*=3. **F**, Q content of q*aro2-mutA* cells containing the indicated YEp352 plasmids or empty vector (-), grown in YNB-p galactose medium with aromatic amino acids (Tyr 15 mg/L). Mean ± s.e.m.; *n*=2 (-), *n*=3 (*ARO2* and *COQ2-MVD1*). ns: no significant difference, *: $P<0.05$, **: $P<0.01$, ****: $P<0.0001$, unpaired two-tailed *t*-test. *n*, number of independent experiments.

Figure S2

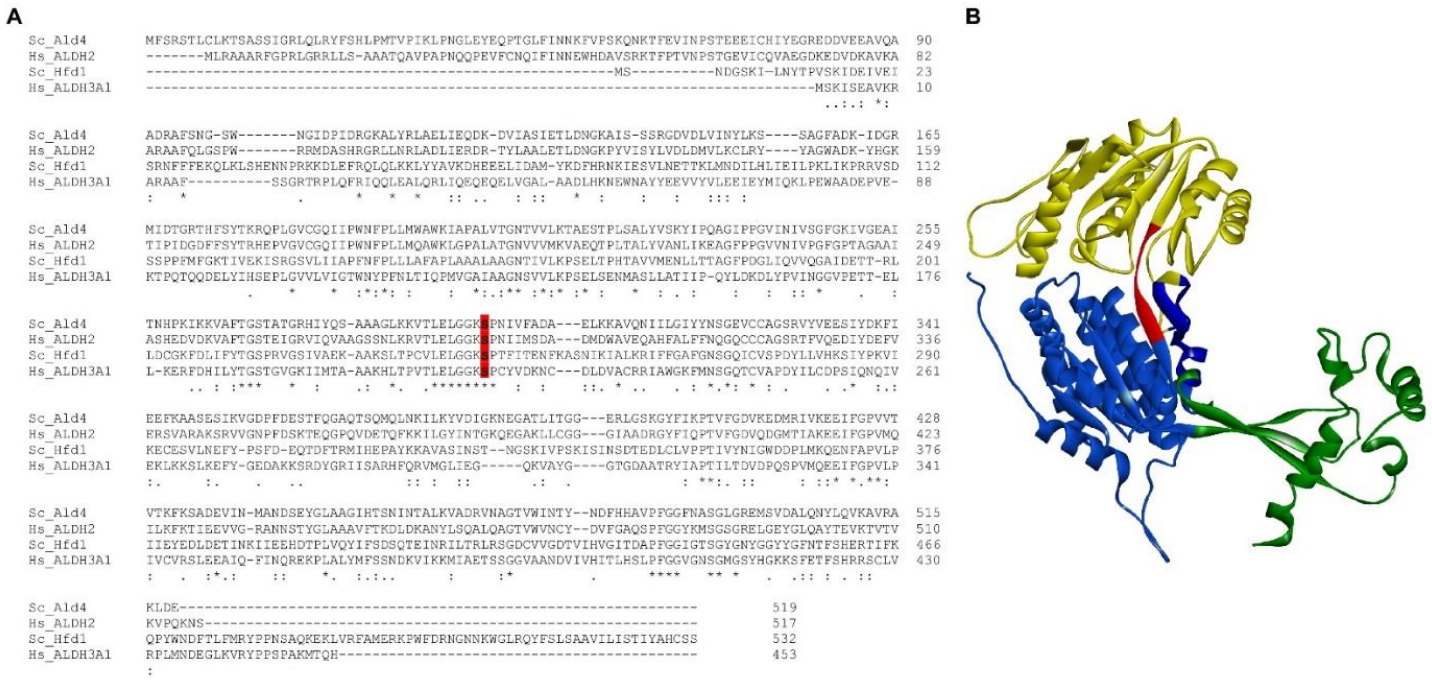

Figure S2 Related to Figure 2: Sequence conservation and structural model of Hfd1.

A, Sequence alignment of Hfd1 and Ald4 from *S. cerevis*iae (UniProt ID, Q04458, P46367, respectively) and ALDH2, ALDH3A1 from *Homo sapiens* (P05091, P30838, respectively). The conserved Ser241 of Hfd1 is highlighted in red. **B**, Homology model of *S. cerevisiae* Hfd1 showing the typical topology of aldehyde dehydrogenases with three domains: the dimerization domain (K103-I127 and H460-end) in green, the NAD binding domain in blue (M1-P102, S128-L237 and H430-S459) and the catalytic domain in yellow (K240-I429). The conserved LELGGKS sequence (L235-S241) that connects the NAD binding domain and the catalytic domain is shown in red.

Figure S3

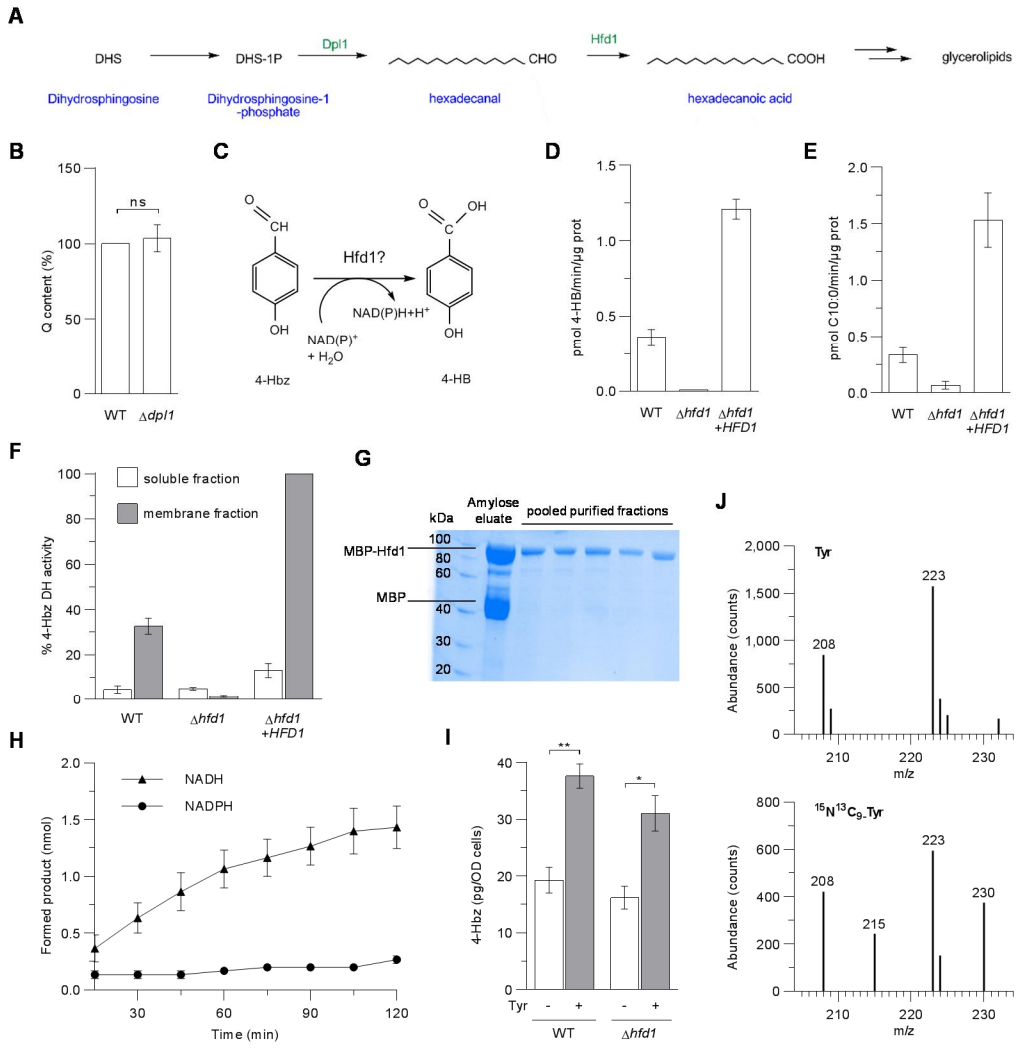

Figure S3 Related to Figure 3: Oxidation of 4-hydroxybenzaldehyde by Hfd1.

A, Dihydrosphingosine degradation pathway in *S. cerevisiae*. **B**, Relative Q content as percentage of WT cells. Mean ± s.e.m.; *n*=6. **C**, Proposed reaction catalyzed by Hfd1. **D**, 4-Hbz dehydrogenase activity measured on total cellular extracts of WT, q*hfd1* cells transformed with pRS415-*HFD1* or empty vector. Mean ± s.e.m.; *n*=3 (WT), *n*=6 (q*hfd1*±*HFD1*). **E**, Decanal dehydrogenase activity measured on extracts described in **S3D**. C10:0, decanoic acid. Mean ± s.e.m.; *n*=3. **F**, Relative 4-Hbz dehydrogenase activity of soluble and membrane fractions as percentage of q*hfd1* cells transformed with pRS415-*HFD1*. Mean ± s.e.m.; *n*=4. **G**, SDS-PAGE of amylose resin eluate and gel filtration fractions containing pure MBP-Hfd1. **H**, Reduction of NAD^+ or $NADP^+$ by MBP-Hfd1 in the presence of 4-Hbz. *n*=3. **I**, 4-Hbz content of cells grown in YNB-p galactose medium containing or not 30 mg/L Tyr. Mean ± s.e.m.; *n*=3. **J**, GCMS spectra of 4-Hbz in extracts of WT cells grown in the presence of 30 mg/L Tyr or ^{15}N $^{13}C_9$-Tyr. Representative spectra from one of three independent experiments are shown. ns: no significant difference, *: $P< 0.05$, **: $P<0.01$, unpaired two-tailed *t* test (**B**), One-way ANOVA test (**I**). *n*, number of independent experiments.

Figure S4

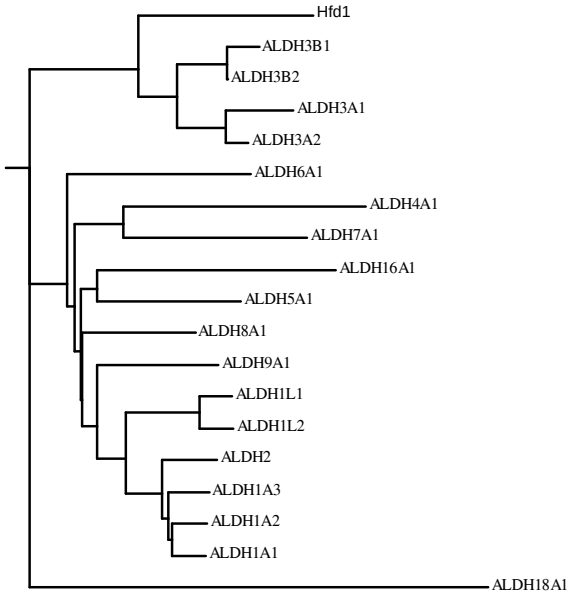

Figure S4 Related to Figure 4: Phylogeny of Hfd1.

Phylogenetic tree of Hfd1 and the 19 human aldehyde dehydrogenase proteins.

SUPPLEMENTAL EXPERIMENTAL PROCEDURES

Chemicals. 4-hydroxybenzoate (4-HB), 4-hydroybenzaldehyde (4-Hbz), para-aminobenzoic acid (pABA), benzaldehyde, decanal, decanoic acid, reduced and oxidized nicotinamide adenine dinucleotide (NADH and NAD^+), NAD phosphate (NADPH and $NADP^+$), methanol, acetonitrile, isopropanol, ethanol, *n*-heptane, trifluoroacetic acid, ethyl acetate, ethyl methanesulfonate (EMS), LC-MS grade formic acid and acetic acid were purchased from Sigma. $^{15}N^{13}C_9$-L-Tyrosine and $^{13}C_9$-L-Phenylalanine were purchased from Cortecnet. 4-HB, 4-Hbz were prepared in water to a final concentration of 1 mM and stored at -20 °C. Tyrosine and phenylalanine stock solutions were prepared in water at 500 mg/L and 10 g/L, respectively, and were sterile filtered and stored at 4 °C. Decanal was prepared in ethanol at a final concentration of 10 mM and stored at -20 °C.

Yeast strains. *Saccharomyces cerevisiae* strains used in this study are listed in the Supplemental Table below. The q*aro8*q*aro9* strain was constructed by crossing q*aro8* and q*aro9* strains and by selecting for the presence of both mutations in a haploid strain after sporulation of the diploid strain according to a published procedure (Sherman, 2002) and tetrad dissection on a Nikon 50i microscope equipped with a micromanipulator. The q*aro8*q*aro9*q*aro2* and q*aro8*q*aro9*q*tyr1* strains were obtained by transforming the q*aro8*q*aro9* strain with the *HIS3* gene amplified by PCR from *Saccharomyces kluyveri* using respectively, Aro2-his3 5ô and Aro2-his3 3ô primers or Tyr1-his3 5ô and Tyr1-his3 3ô primers (see Supplemental Table) and by selecting His prototroph clones. The q*tyr1* strain was created similarly by transforming the BY4741 strain. The q*coq6*q*hfd1* strain was constructed by crossing q*coq6* and q*hfd1* strains and by selecting for the

presence of both markers associated to the respective deletions in a haploid strain after tetrad dissection. In all cases, the integration of the deletion cassette was verified by PCR amplification of the locus on the genomic DNA. Transformations were performed using the lithium acetate method (Burke et al., 2000).

Supplemental Table: Yeast strains used in this study

Strain	Genotype	Source
BY4741 / WT	*Wild Type, MATa his3*φ*1 leu2*φ*0 met15*φ*0 ura3*φ*0*	Euroscarf
φ*aro2*	*MAT*α *his3*φ*1 leu2*φ*0 lys2*φ*0 ura3*φ*0 aro2::kanMX4*	Euroscarf
φ*aro2*	*MATa his3*φ*1 leu2*φ*0 met15*φ*0 ura3*φ*0 aro2::kanMX4*	Euroscarf
φ*aro8*	*MATa his3*φ*1 leu2*φ*0 met15*φ*0 ura3*φ*0 aro8::kanMX4*	Euroscarf
φ*aro9*	*MAT*α *his3*φ*1 leu2*φ*0 lys2*φ*0 ura3*φ*0 aro9::kanMX4*	Euroscarf
φ*aro8*φ*aro9*	*MATa his3*φ*1 leu2*φ*0 ura3*φ*0 aro8::KanMX4 aro9::KanMX4 met15*φ*0*	This study
φ*aro2-mutA*	*MATa his3*φ*1 leu2*φ*0 met15*φ*0 ura3*φ*0 aro2::kanMX4 hfd1-C722T*	This study
φ*tyr1*	*MATa his3*φ*1 leu2*φ*0 met15*φ*0 ura3*φ*0 tyr1:: SkHIS3*	This study
φ*aro8*φ*aro9*φ*aro2*	*MATa his3*φ*1 leu2*φ*0 ura3*φ*0 aro8::KanMX4 aro9::KanMX4 met15*φ*0 aro2::SkHIS3*	This study
φ*aro8*φ*aro9*φ*tyr1*	*MATa his3*φ*1 leu2*φ*0 ura3*φ*0 aro8::KanMX4 aro9::KanMX4 met15*φ*0 Tyr1::SkHIS3*	This study
φ*hfd1*	*MATa his3*φ*1 leu2*φ*0 met15*φ*0 ura3*φ*0 hfd1::kanMX4*	Euroscarf
φ*coq6*	*MAT***Ŭ***coq6::LEU2 trp1-1 can1-100 ura3-1 ade2-1 his3-11,15*	(Gin et al., 2003)
φ*coq6*φ*hfd1*	*MAT? ura- his- met- lys- trp? met? coq6::LEU2 hfd1::kanMX4*	This study

Growth assay on plates. Overnight cultures in YNB-p 2% galactose were diluted in water to OD_{600} = 1 and ten-fold serial dilutions in sterile water were performed in 96 well plates. 5 µL of each dilution was spotted on YNB-p solid medium containing either glucose (Glu) or LG. Plates were imaged after incubation at 30 °C for three days (Glu) or five days (LG).

EMS mutagenesis and genetic analysis of φ*aro2-mutA*. EMS mutagenesis was carried out essentially as described (Winston, 2008). A culture of 10 mL of φ*aro2* cells (MATa) in YNB-p LG medium at OD_{600} 1.2, was centrifuged at 5,000 g for 30 sec. The cells were rinsed twice with water and resuspended in 2.5 mL 0.1 M sodium phosphate buffer pH 7.0. 80 µL EMS was added and the cells were incubated for 1 h at 30 °C, 200 rpm. The cells were harvested by centrifugation at 5,000 g for 30 sec, rinsed three times in 1 mL 5% (w/v) sodium thiosulfate and finally resuspended in 1 mL water. The cells were diluted 1,000 fold in water and 120 µL were spread on YPD plates. After two days, colonies (~1,000 / plate, ~50,000 colonies in total) were replica plated onto YNB-p glucose medium using sterile velvets and grown for 24 h at 30 °C. The cells were then replica plated onto YNB-p LG medium containing or not 10 µM 4-HB. After 4 days at 30°C, the plates were compared visually and clones that grew exclusively on YNB-p LG medium containing

4-HB were selected and their phenotype was verified by streaking on YNB-p LG medium containing or not 10 µM 4-HB. Only one clone, cp*aro2-mutA*, exhibited the desired phenotype. cp*aro2-mutA* was mated with the cp*aro2* strain (MATŬ) and diploids were selected on YNB glucose medium lacking lysine and methionine. The diploid strain was grown in YPD medium and was then sporulated to produce meiotic progeny. Spores from 20 tetrads showed 2:2 segregation for respiratory growth on YNB-p LG medium implying mutation at a single locus. One clone unable to grow on YNB-p LG medium was transformed with a yeast genomic DNA library previously described (Pierrel et al., 2007). Transformants were screened for growth on YNB-p LG medium. Plasmids from positive clones (YEp352-*ARO2*, YEp352-*HFD1* and YEp352-*COQ2-MVD1*) were recovered in *E. coli* TOP10 by transforming yeast genomic DNA and selecting on LB-agar medium containing ampicillin. Plasmids were then purified and sequenced.

Plasmid construction. Plasmids used in this study are listed in the Supplemental Table below. The centromeric plasmid pRS415 was used to construct pRS415-*HFD1* by cloning a PCR product corresponding to the *HFD1* gene with its own promoter and terminator obtained with the primers XhoI-hfd1 and NotI-hfd1 (see Supplemental Table) and genomic DNA from the BY4741 strain as template. pRS415-*HFD1-S241L* was obtained similarly except that genomic DNA from the cp*aro2-mutA* strain was used as template in the PCR reaction. *E. coli UBIC* gene was amplified by PCR from the genomic DNA of the MG1655 strain using the primers 5EcoRI-ubiC and 3XbaI-ubiC. The fragment was cloned at the EcoRI and XbaI sites of pBADIK (Py et al., 1999) and was then subcloned into pRS426-M25C1 using the EcoRI and HindIII restriction sites to obtain pRS426-*UBIC*. pMAL-c2-*HFD1* was obtained by ligating at the BamH1 and SalI sites of pMAL-c2 a digested PCR product obtained by amplifying the *HFD1* gene from the genomic DNA of the BY4741 strain. pMAL-c2-*HFD1-S241L* was obtained similarly except that the PCR reaction was performed on the genomic DNA of the cp*aro2-mutA* strain. *E. coli* TOP10 cells were used for cloning and plasmid amplification, the plasmids were purified with a standard miniprep kit (EZ-10, Euromedex) and sequencing was used to confirm all cloning products.

Supplemental Table: Plasmids used in this study

plasmid	Description	source
pRS415	Centromeric vector, *lac* promoter , Amp^r, *LEU2*	(Sikorski and Hieter, 1989)
pRS415-*HFD1*	pRS415, Hfd1	This study
pRS415-*HFD1-S241L*	pRS415, Hfd1-S241L	This study
pBADKI-*UBIC*	pBADKI containing *E. coli UBIC* ORF	This study
pRS426-*M25C1*	Episomal vector containing the *MET25* promoter and the *CYC1* terminator, *URA3*, *Amp^r*	(Mumberg et al., 1995)
pRS426-*UBIC*	pRS426-M25C1 containing *E. coli UBIC* under the control of the *MET25* promoter and the *CYC1* terminator	This study
pMAL-c2-*HFD1*	pMAL-c2, Hfd1	This study
pMAL-c2-*HFD1-S241L*	pMAL-c2, Hfd1-S241L	This study
YEp352	Episomal vector, *URA3*, *Amp^r*	ATCC
YEp352-*ARO2*	YEp352 containing the sequence 226031-227968 of chromosome VII encompassing the *ARO2* gene	This study

YEp352-*COQ2-MVD1*	YEp352 containing the sequence 700373-703089 of chromosome XIV encompassing the *COQ2* and *MVD1* genes	This study
YEp352-*HFD1*	YEp352 containing the sequence 490122-492366 of chromosome XIII encompassing the *HFD1* gene	This study
p*COQ8*	pRS423 containing *S. cerevisiae COQ8* under the control of its own promoter	(Ozeir et al., 2015)
pNK5	pAKNF316 encoding 3xFLAG-ALDH3A2	(Nakahara et al., 2012)
pNK10	pAKNF316 encoding 3xFLAG-ALDH3A1	(Kitamura et al., 2013)
pNK12	pAKNF316 encoding 3xFLAG-ALDH3B1	(Kitamura et al., 2013)
pNK14	pAKNF316 encoding 3xFLAG-ALDH3B2	(Kitamura et al., 2013)

The chromosomal coordinates indicated for the inserts of the YEp352 plasmids are from the S288C strain (http://www.yeastgenome.org).

Supplemental Table: Primers used in this study

Primer	Sequence
BamH1-hfd1	GAATTCGGATCCATGTCAAACGACGGCTC
NotI-hfd1	CACTAAGCGGCCGCCTCAAAACAGGGATGTTCCTAAACCCG
SalI-hfd1	CTGACGTGTCGACTCAGGAAGAACAATGAGCG
XhoI-hfd1	ATCCTGCCTCGAGGAGGAAATGGAACAACGAATTTCCAGCC
5EcoRI-ubiC	TATCGAATTCATGTCACACCCCGCGTTAACGCAACTG
3XbaI-ubiC	CTTCCGTCTAGATTAGTACAACGGTGACGCC
Aro2-his3 5ô	GCGTTATTCTCATCGTATAGTATCGAAAAAAGAAAATAGTATC ATAGCACAGAGGC**ATGACAGAACCAGCCCAAAAAAAGC**
Aro2-his3 3ô	ACATATACATGCGTATATAAATATACATAACTCTTGAGGGGTT TTGTTTCTATCT**TCACATCAAAACACCTTTGGTTGAGGG**
Tyr1-his3 5ô	CAAGAATACCGTAGCACTTGAAGGAAAGAGGACAGCATATCC **ATGACAGAACCAGCCCAAAAAAAGC**

Tyr1-his3 3ô	GGGCATTTGTCACAATATATATTTTTATTCAGTTATATAAATAT ACTCC**TCACATCAAAACACCTTTGGTTGAG**

Nucleotides written in bold correspond to the sequence of the *HIS3* gene from *Saccharomyces kluyveri*.

Decanal dehydrogenase activity assay. The assay was similar to that described for 4-Hbz except that yeast extracts were incubated with 100 µM decanal instead of 4-Hbz for 10 min. The extraction procedure of decanoic acid (C10:0) was modified from a method described elsewhere (Neuber et al., 2014). Briefly, 500 µL of isopropanol/*n*-heptane/2 M trifluoroacetic acid (40:10:1, v/v/v) was added to the samples with 10 µL of 10 µM pentadecanoic acid (C15:0) used as an internal standard. After vortexing for 1 min, 200 µL of *n*-heptane and 300 µL of water were added. After vortexing for 1 min, tubes were incubated on ice for 10 min and centrifuged at 400 g for 5 min. 200 µL of the upper phase was transferred into a new tube. The extraction was repeated with 200 µL of *n*-heptane and the upper phase was collected and pooled with the first one. After evaporation under nitrogen at 37 °C, samples were resuspended in ethanol for HPLC-MS analysis (U3000 Dionex and Thermofisher MSQ Plus mass spectrometer). Separation was performed on a C18 column (Betabasic-18, 5 µm, 4.6 x 150 mm, Thermo Scientific). Two mobile phases were used for elution at a flow rate of 0.5 mL/min: water (A) and 0.05% (v/v) acetic acid in methanol (B). The linear gradient profile was 0-4 min, 60% B; 4-11 min, 60-100% B; 11-21 min, 100% B; 21-22 min, 100-60% B; 22-27 min, 60% B. Commercial decanoic acid was used to optimize separation and MS detection. The MS spectrometer was operated in electrospray negative ion mode (cone voltage 70 V and 90 V for C10:0 and C15:0, respectively, 450 °C) and peaks obtained in single ion monitoring, m/z 171.3 (C10:0) and m/z 241.3 (C15:0), were used for quantification.

Purification and activity assay of MBP-Hfd1. *E. coli* Rosetta II cells containing pMAL-c2-*HFD1* were cultured in 4 L LB medium supplemented with ampicillin (100 µg/mL) and 2% glucose until OD_{600} ~ 0.5, at which point 1 mM IPTG was added. The culture was shifted to 17 °C and incubated overnight at 200 rpm. Cells were harvested by centrifugation at 4,000 rpm, 4 °C, 20 min, then washed with cold water and centrifugation was repeated. The cell pellet was stored at -80 °C. Cells were resuspended in 20 mL buffer A (20 mM Tris-HCl pH 7.4, 200 mM NaCl, 1 mM EDTA), lysed by sonication (5 min on ice, 10 s on/off pulses) and centrifuged at 100,000 g for 45 min at 4 °C. The supernatant was deposited on amylose resin (2 mL, New England Biolabs) equilibrated with buffer A, the column was washed with 30 mL buffer A and the protein was eluted with buffer A containing 50 mM maltose. MBP-Hfd1 was concentrated by centrifugation with Centricon 50 (Millipore) and 2 mL were loaded onto a Sephadex 200 column equilibrated with 20 mM Tris-HCl pH 7.4, 200 mM NaCl. Fractions were analyzed by SDS-PAGE and those containing MBP-Hfd1 were pooled and concentrated with Centricon 50. 10% glycerol was added to the purified protein before storing at -80 °C. Purified MBP-Hfd1 (5-15 µg) was incubated with 500 µM NAD^+ and 100 µM substrate (4-Hbz or benzaldehyde) in PIPES 50 mM pH 7.1 at 30 °C, total volume 100 µL. The reaction was monitored by measuring the fluorescence of NADH produced by the reduction of NAD^+ (excitation at 356 nm and emission at 460 nm) in a Tecan infinite M200. A linear standard curve, obtained with 0, 1, 2.5, 5 and 10 nM NADH was used to quantify the production of NADH in the assay.

SUPPLEMENTAL REFERENCES

Burke, D., Dawson, D., and Stearns, T. (2000). In Methods in Yeast Genetics (Cold Spring Harbor Laboratory Press, Plainview, NY).

Gin, P., Hsu, A.Y., Rothman, S.C., Jonassen, T., Lee, P.T., Tzagoloff, A., and Clarke, C.F. (2003). The *Saccharomyces cerevisiae COQ6* gene encodes a mitochondrial flavin-dependent monooxygenase required for coenzyme Q biosynthesis. J. Biol. Chem. *278*, 25308-25316.

Kitamura, T., Naganuma, T., Abe, K., Nakahara, K., Ohno, Y., and Kihara, A. (2013). Substrate specificity, plasma membrane localization, and lipid modification of the aldehyde dehydrogenase ALDH3B1. Biochim. Biophys. Acta *1831*, 1395-1401.

Mumberg, D., Muller, R., and Funk, M. (1995). Yeast vectors for the controlled expression of heterologous proteins in different genetic backgrounds. Gene *156*, 119-122.

Nakahara, K., Ohkuni, A., Kitamura, T., Abe, K., Naganuma, T., Ohno, Y., Zoeller, R.A., and Kihara, A. (2012). The Sjogren-Larsson syndrome gene encodes a hexadecenal dehydrogenase of the sphingosine 1-phosphate degradation pathway. Mol. Cell *46*, 461-471.

Neuber, C., Schumacher, F., Gulbins, E., and Kleuser, B. (2014). Method to simultaneously determine the sphingosine 1-phosphate breakdown product (2E)-hexadecenal and its fatty acid derivatives using isotope-dilution HPLC-electrospray ionization-quadrupole/time-of-flight mass spectrometry. Anal. Chem. *86*, 9065-9073.

Ozeir, M., Pelosi, L., Ismail, A., Mellot-Draznieks, C., Fontecave, M., and Pierrel, F. (2015). Coq6 Is Responsible for the C4-deamination Reaction in Coenzyme Q Biosynthesis in Saccharomyces cerevisiae. J. Biol. Chem. *290*, 24140-24151.

Pierrel, F., Bestwick, M.L., Cobine, P.A., Khalimonchuk, O., Cricco, J.A., and Winge, D.R. (2007). Coa1 links the Mss51 post-translational function to Cox1 cofactor insertion in cytochrome c oxidase assembly. EMBO J. *26*, 4335-4346.

Py, B., Loiseau, L., and Barras, F. (1999). Assembly of the type II secretion machinery of Erwinia chrysanthemi: direct interaction and associated conformational change between OutE, the putative ATP-binding component and the membrane protein OutL. J. Mol. Biol. *289*, 659-670.

Sherman, F. (2002). Getting started with yeast. Methods Enzymol. *350*, 3-41.

Sikorski, R.S., and Hieter, P. (1989). A system of shuttle vectors and yeast host strains designed for efficient manipulation of DNA in *Saccharomyces cerevisiae*. Genetics *122*, 19-27.

Winston, F. (2008). EMS and UV mutagenesis in yeast. Current Protocols in Molecular Biology *13*, 3B1-3B5.